Dear Editor,

Please find the revised manuscript of the research article egusphere-2023-1947.

In this document, we have attached our responses to the two reviews. The track-changes version of the manuscript is available at the end. Added text is shown in blue underlined, while removed text in shown in red strikeout.

Please also note, that we have corrected the values of inner and outer radii used in Section 3.5. Indeed, we only realized after submitting the response to the referees that the numbers initially given in the manuscript did not exactly correspond to those used in the simulations and in Figure 1. This modification does not change the results or conclusions of Section 3.5 on the validation of the workflow.

Kind regards
Anna Braun on behalf of all co-authors

Response to RC1 from Z.R. Courville on egusphere-2023-1947

We are thankful to Z.R. Courville for thorough and constructive review of our manuscript.

We have copied the comments of Z.R. Courville in blue. Our corresponding responses are available in black below each comment and proposed modifications to the manuscripts are written in yellow highlighted italics. The bold text line numbers correspond to the original manuscript.

Best regards

Anna Braun on behalf of all co-authors

The manuscript presents a very interesting physically-based modeling approach to the evolution of snow specific area during temperature gradient metamorphism, notably presenting results constraining the kinetic attachment coefficient, which is difficult to measure and has proved an elusive parameter in overall efforts at understanding temperature gradient metamorphism. I found the result that the kinetic coefficient varied between the two samples, and then over the course of one of the experiments particularly interesting, but intuitively makes sense in terms of the dependence of the kinetic coefficient on the morphology of snow grains. I also find the SSA modeling results presented in Fig 6 compelling with respect to the microCT data, with the match between model and experimental results remarkable. The manuscript is very well written. Below, I offer a few minor suggestions for consideration to improve clarity for a reader. The main suggestion I have is to use a consistent definition of alpha throughout the text. I also had a few questions about the specifics of the model mentioned that I think might warrant clarification.

Thanks a lot for the positive feedback. We are encouraged to confirm the intuitive understanding of temperature gradient metamorphism by a rigorous numerical approach. As detailed below, we will improve the naming of alpha, consistently calling it “condensation coefficient”.

Line 64: “at the downside” is not quite the right phrase, I would suggest “at the expense” instead

We will change **Line 64** accordingly:

“[…], at the expense of microstructural realism.”

Line 73: I would suggest writing: “While the interfacial curvature is a geometrical quantity, the interface growth velocity must be computed from a physical model.” That is only a suggestion to make that sentence clearer vs. “first” and “second” term since that sentence has a lot of terms in it, and that’s if I’ve interpreted the sentence correctly.

The sentence will be rewritten in the revised manuscript, removing the words “first” and “second”. We also modified the sentence following a comment from Thomas Kaempfer. We will rephrase the text **Line 73** to:

“While the interfacial curvature is a purely geometrical quantity that can directly be computed from a µCT image, v_n is a physical quantity that further depends on the involved physical processes.”

Line 88: I’m not sure “motion” is the best term for the interface, and would suggest “evolution” or maybe “migration” instead.

We propose to change **Lines 87-88** using the term “evolution”:

“For an arbitrary snow structure, morphological changes during metamorphism are predominantly driven by the coupled diffusion of heat and mass together with ice-air interface evolution due to deposition and sublimation of vapor.”

We will further rephrase “motion of the interface” in **Lines 92-93**:

“Due to the separation of time scales between heat and mass diffusion in the pores and the evolution of the interface due to crystal growth, [...]”

Line 89: How was the size of the representative snow volume determined? (or is that in the Pinzer article? If they do discuss how the representative volume was determined, I would mention that briefly.)

Following the reviews, we have performed additional simulations determining a representative elementary volume with respect to the growth rate.

In the figure below, the sample sizes used in the article correspond to the largest volumes for each sample. This shows that the estimated growth rates using these sample sizes are representative.

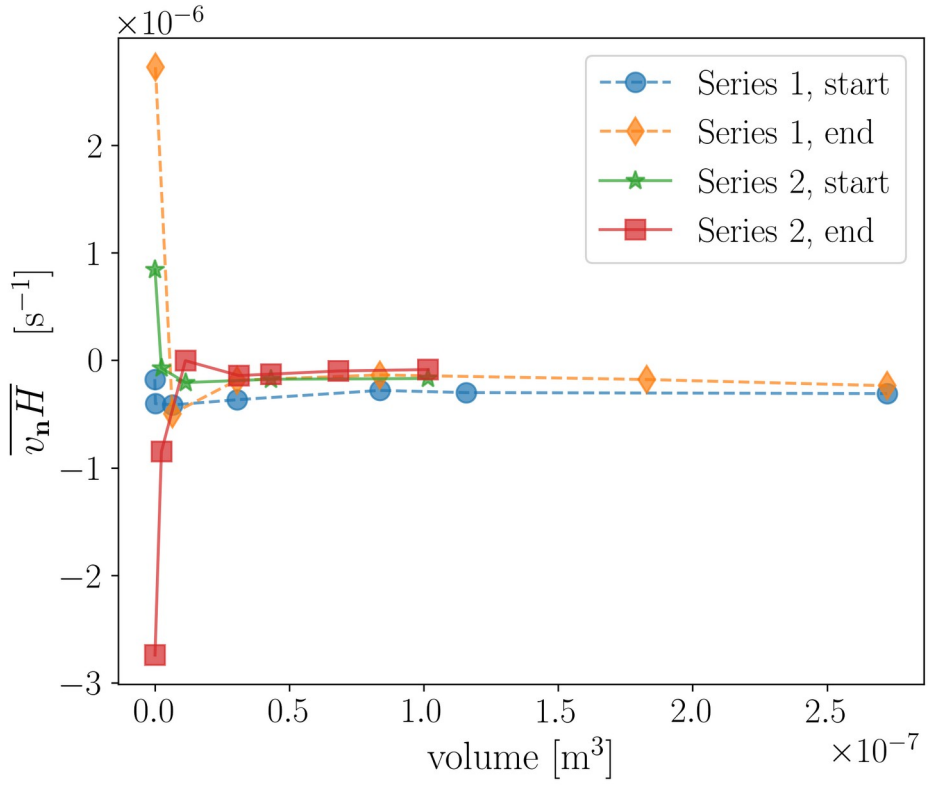

We will discuss this result, starting **Line 179**:

“The FE meshes of this article are based on the whole available µCT images. We verified that these selected volumes were large enough to yield representative results.. By varying sub-volumes extracted from the center of µCT images at the start and the end of both series ($I(t_1)$, $I(t_{49})$, $\hat{I}(t_1)$ and $\hat{I}(t_{83})$), we found that the simulated growth rate corresponds to a representative value for the sample sizes used in this study. This is consistent with the results of Calonne et al. (2011) for thermal conductivity, that report representativeness for sample side-lengths between 2.5 and 5mm.”

Line 115: Throughout the text, there are several definitions/names of the parameter alpha (or at least I think they are all referring to alpha). As a suggestion, I recommend either being more consistent, or explaining at the first instance that alpha has been called different things. The first time it happened, I was wondering why the change from “vapor attachment coefficient” to

"condensation coefficient", and recommended defining alpha as "the vapor attachment coefficient, or the condensation coefficient" at the first definition of alpha, but then I noted that there are several different forms of the definition used throughout the manuscript, including "kinetic coefficient" (line 293) and "attachment kinetics coefficient" (line 297). Again, I **think** these are all referring to alpha, but I am not sure.

We will introduce alpha in **Lines 39** and refer to it as the "condensation coefficient". We will also mention that other names of alpha appear in the literature:

"In this picture, one key parameter driving snow metamorphism is the condensation coefficient α, also called attachment, kinetic or sticking coefficient (Libbrecht, 2005; Kaempfer & Plapp, 2009; Krol & Loewe, 2016; Demange et al., 2017b; K. Fourteau et al., 2021a; L. Bouvet et al., 2022) that controls the kinetics of vapor deposition and sublimation."

We will further call alpha "condensation coefficient" in abstract (**Line 8**) and throughout the text.

Line 119: Ditto that last comment for the definition of alpha in this instance (I stopped noting all the different terms used for alpha as I went on in my review, see the above comment. I think either calling it the same thing or discussing all the different variations is warranted to alleviate confusion.)

We will change it according to the response to the previous comment.

Line 119: Suggest rewriting as "the kinetic coefficient α is defined as the probability of a water molecule sticking to an impinging surface." (this is only a minor grammar/usage suggestion)

From what we understand, the word impinging applies to the molecule rather than to the surface. We propose to rephrase **Line 119** as:

"In the Hertz-Knudsen equation, the condensation coefficient α is defined as the probability of a water molecule sticking to a surface after impinging on it."

Line 123: Is (7) referring to a reference in bibtex or some other citation managing software? Or is it referring to equation 7? Might be clearer if it said "eq. 7"

This should be a reference to Eq. 7. We will change **Line 123** accordingly:

"[…] as deviations from the local constitutive behavior (Eq. (7)) due to non-local surface processes (Libbrecht, 2005)."

Line 145: By "shorter" does that mean the sample is physically smaller, or that the time was shorter (I mean, I think I know the answer since the hours are greater for Series 2)? Suggest rewriting to clarify, maybe "Series 1 lasted 384 h and had a shorter sample height…" if that is what is meant. Also seems like the sample thicknesses/heights should be included as a well as the temperature gradients, even if the details are in the Pinzer paper.

No, just the duration is shorter. We will change **Line 145** to avoid confusion:

"Series 1 lasted 384 h, while Series 2 lasted 665 h."

We will further correct and rephrase **Line 155**, including the size of the samples:

"This corresponds to samples of 7.5x7.5x4.9mm^3 for series 1 and 5.4.x5.4x3.5mm^3 for series 2."

Line 146: Does mean T refer to the average air/ambient temperature for the experiment or the average temp throughout the sample?

Here, we mean the mean temperature throughout the sample. We will change **Line 146** accordingly:

"The mean temperature T of the sample [...]"

Line 159: How was "a reasonable volumetric division" determined or quantified? Specify the requirements.

The main requirement of the mesh beside preserving the surfaces is the achievement of the accurate discretized numerical solution. There is no clear cut-off value here, apart from the general idea that the elements need to be small compared to the length-scale of the physical problem to be solved and that smaller elements *usually* yields less errors. A further constraint of the element size is the available computational power, as smaller elements means more elements.

We will rephrase **Lines 159-160** to be more specific:

"The production of an appropriate mesh that discretizes the air and ice domains, preserves the ice-air interface, and is fine enough to get accurate numerical solution (without overloading computational resources) is a key requirement for our problem."

To ensure that we used a sufficient degree of refinement, we have performed additional simulations with different degrees of refinement. This provides information about the sensitivity of our results to the FE mesh. As can be seen from the graph below (stars represent the number of elements that were used in the manuscript), the growth rate v_nH is only reasonably impacted when increasing the number of elements. Moreover, as discussed later, the very good agreement between a FE simulation and the analytical solution for a spherical problem suggests that our meshing criteria yields an appropriate mesh. This will be stated **Line 170**:

"We have estimated the sensitivity of our results to the FE mesh. We found that doubling the number of elements in the mesh impacted the growth rate by about 10%. This is small in light of the dependence of the SSA values on the condensation coefficient α investigated in this study. Moreover, the very good agreement between a FE simulation and the analytical solution for a spherical problem (see Sect. 3.6) suggests that our meshing criteria yield an appropriate mesh."

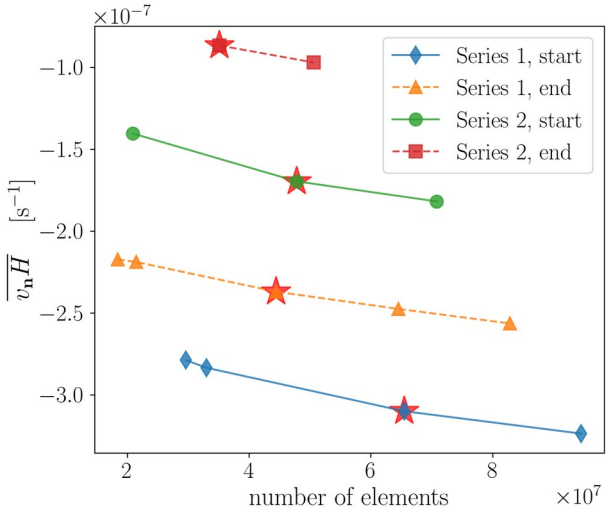

Line 165: Likewise, define “small air padding” quantitatively, or if dependent on the size of the volume of interest/SSA or sample grain size, describe how that was determined.

The thickness of the air-padding layer is 3 voxels around the 300x300x196 snow image. This will be specified in the text **Line 160**:

“To this end, we employ the open-source Computational Geometry Algorithms Library (CGAL) (The CGAL Project, 2022). Specifically, we use the class Polyhedral_mesh_domain_with_features_3 that implements a tetrahedral mesh of a domain bounded by polyhedral surfaces that are preserved. The provided surfaces need to be closed and free of self-intersections. To obtain such surfaces, we extract the ice-air interface from the binary µCT data (Eq. (11) and (12)) following the procedure from (Krol and Löwe, 2018), namely by applying a Gaussian smoothing and the contour filter from the Visualization Toolkit (VTK) (Schroeder et al., 2006). However, by default this procedure applied to µCT images yields a surface that is open at the boundaries of the domain. In order to obtain closed surfaces, we added a small air-padding (three voxel-thick) around the image. This allowed us to properly define a closed outer boundary suitable for meshing. As detailed below, we provided special care to ensure that the introduction of this artificial air-padding does not perturb the simulation within the snow microstructure itself.”

Line 189: For readers not familiar with Elmer, it would be good to add a brief description of what an ILU preconditioner is or does. I will note, though, that in general the authors have done a very good job of describing what the different functions in Elmer are for a non-Elmer user.

We will add a reference for the ILU preconditioner in **Line 188**:

“The equations are solved with the iterative biconjugate gradient stabilized method (BiCGSTAB; Van der Vorst, 1992) together with an ILU preconditioner, meant to facilitate the numerical solving by performing an incomplete LU factorization (Saad, 1996).”

Line 263: I would put in the length scale of the test case (0.9 mm) so the reader doesn’t have to do the math, i.e., “In this way, the length scales of the test case (0.9 mm for the outer radius) are a similar order of magnitude…”

We add the lengths of the inner and outer radii **Line 264**:

“where the inner radius is set to R=21 voxel and the outer radius set to R_{\infty}=51 voxel with a voxel size of 18µm, corresponding to inner and outer radii of 0.38 and 0.92mm, respectively.”

Figure 1. Suggest putting a scale bar in for the sphere (in mm) if it doesn’t clutter the figure too much since that will help a reader compare to typical snow grain sizes, or adding the outer sphere dimension to the caption.

We will add a scale bar to the Figure 1b. The revised Figure is displayed below.

Figure 1. For b) is the blue the “air padding” similar to what was added to the microCT volume?

The blue color in the Figure 1b does not correspond to an air-padding layer but to the outer sphere. It is blue as vapor sublimates from the outer sphere. We will state that more clearly in the caption of the Figure 1:

"Figure 1. [...] b) Clip of the outer and inner spherical shells with visible elements colored by the interface velocity v_n (sublimation in blue, deposition in red)."

Moreover, we will extent the text in **Lines 270** to discuss where sublimation and deposition occur:

"*After solving the vapor equation, with appropriate boundary conditions, we obtain the interface velocity v_n, shown in Fig.1b. As expected, we observe a positive velocity on the inner shell, corresponding to vapor deposition, and a negative velocity on the outer shell, corresponding to sublimation.*"

Figure 1. For c) what are the red and blue dashed lines showing? I'm guessing that is the (sim-theo)/theo for values of alpha, but that should be called out in the legend, and which axis those values are plotted on should be indicated for easy of reading.

Indeed, the red and blue dashed lines corresponds to the relative errors.

This will be mentioned in the caption of **Fig. 1**:

"Figure 1. [...] c) Comparison of the growth rate v_nH on the inner radius R of theoretical (theo) and simulated (sim) solution of the spherical shell test case for different values of the condensation coefficient α. Two different surface mesh qualities with (smooth) and without (non-smooth) smoothing are employed. The red dots, blue squares and black solid line correspond to v_nH on the left y-axis while the dashed red and blue lines correspond to simulation error on the right y-axis."

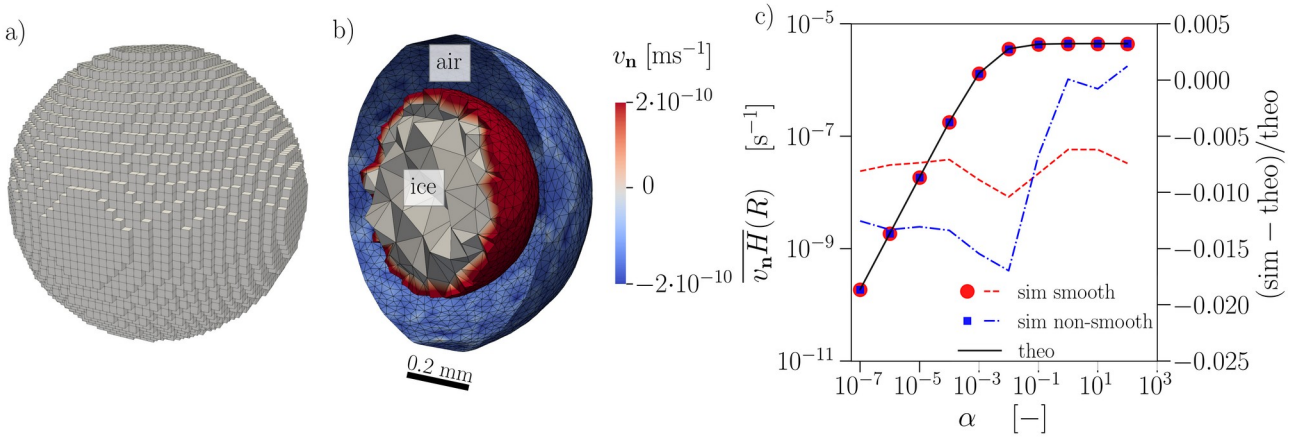

Line 308: what does the RMSE minimum "is deeper" mean? That the RMSE minimum is lower?

We will replace "deeper" with "lower" **Line 308** to:

"[…] the RMSE minimum for Series 2 is lower despite higher data scattering."

Line 311: Should be "a time step refined down to the time interval between two microCT images…" or something (seems like there is a missing preposition after "down").

We will change **Line 311** accordingly:

"[…] we performed simulations with a time step refined down to the time interval between […]."

ADDITIONAL REFERENCES:

Demange, G., Zapolsky, H., Patte, R., & Brunel, M.: A phase field model for snow crystal growth in three dimensions, Npj Computational Materials, 3(1), 1–7, https://doi.org/10.1038/s41524-017-0015-1, 2017b.

Saad, Y.: Iterative Methods for Sparse Linear Systems, Society for Industrial and Applied Mathematics, 2003.

Response to RC2 from Thomas Kaempfer on egusphere-2023-1947

We are thankful to Thomas Kaempfer for thorough and constructive review of our manuscript.

We have copied the comments from annotated PDF of the review, with the corresponding text line numbers, below in blue. Our responses are available in black below the comments. Proposed modifications to the manuscript are given in yellow highlighted italics. The bold text line numbers correspond to the original manuscript.

Best regards

Anna Braun on behalf of all co-authors

The paper presents a novel approach to model the evolution of the specific surface area (SSA) during temperature gradient metamorphism (TGM). It uses X-ray micro-computed tomography (mu-CT) images of snow in combination with a numerical solution of steady-state energy and mass conservation equations at the micro-structural scale and a surface area equation based on physics first principles. The only "free" parameter in the model is the vapor attachment coefficient alpha and it is proposed that SSA evolution can be predicted using an adequately chosen "effective" alpha.

The paper is generally well written with a strong emphasis on the numerical solution and analysis of error propagation. The strength and limitations of the approach are clearly presented.

Clarity could be improved by using more concise language and unified terminology (see minor comments in annotated PDF-file). The paper could further benefit by considering the following specific remarks. I suggest the paper to be revised accordingly before accepting it for publication.

Specific remarks

1. Introduction, line 36ff: While it is OK to quickly concentrate on the relevant mechanisms for the TGM situation studied in this paper (energy and mass conservation, attachment kinetics), I suggest justifying why other processes are of second order instead of "boldly" postulating that it is all about alpha.

It is indeed true that while heat and vapor diffusion together with vapor attachment kinetics are usually the processes used to study snow metamorphism from the pore scale, other processes (such a mechanical deformation or air advection) might interact metamorphism and the temporal evolution of the SSA. This will be clarified in the introduction by adding text **Line 36:**:

"Physical models of snow metamorphism must comply with the ice crystal growth dynamics at the pore scale (Krol and Löwe, 2016), which includes heat and vapor diffusion, accommodated by attachment kinetics controlling the deposition and sublimation of water molecules onto the ice lattice (Colbeck, 1983; Libbrecht, 2005). Secondary effects on the temporal SSA evolution might be expected from other processes like mechanical deformation (Wang and Backer, 2013; Schleef et al., 2014), advection of air in the porosity (Ebner et al., 2016, Jafari et al., 2022). In this picture, one key parameter driving snow metamorphism is […]".

We also propose to change the first paragraph of Sect. 2.1, **Lines 87-94** and explain that our motivation to neglect the potential influence of mechanics and air movement is twofold: (i) it corresponds to the basic mechanisms used to explain metamorphism in the most of the literature and is thus a good candidate in terms of minimum-required complexity, and (ii) it is consistent with the set-up under which the experimental data were acquired:

“For an arbitrary snow structure, morphological changes during metamorphism are predominantly driven by the coupled diffusion of heat and mass together with ice-air interface evolution due to deposition and sublimation of vapor. In the following, we closely follow the descriptions by Kaempfer et al., (2009), Calonne et al., (2014), Krol and Loewe (2016), and Fourteau et al. (2020). We consider a representative snow volume at the micro-scale consisting of ice and air and denote the sub-domains occupied by the ice and air phase by Ω_i and Ω_a, respectively. In the following, subscripts i and a denote quantities which are defined in the respective domains Ω_i and Ω_a. Due to the separation of time scales between heat and mass diffusion in the pores and the evolution of the interface due to crystal growth, we employ the common assumption of small particle Péclet number (Libbrecht, 2005) and consider stationary heat and mass diffusion equations. Furthermore, we neglect the influence of mechanical deformation, as usually done in pore-scale metamorphism models (e.g., (Calonne et al., 2014b; Krol and Löwe, 2016)). We also neglect the potential presence of convection and air advection in the pore space. These assumptions are consistent with the experimental data used here, obtained under controlled laboratory conditions (Pinzer et al., 2012). They are also good candidates in terms of minimum-required complexity to model SSA evolution from pore-scale physics. The partial density of water vapor […]”.

2.Presentation of the approach (e.g., Introduction, lines 70ff; or beginning of section 3, lines 159ff – possibly add a new sub-subsection at the beginning of sub-section 3.2): The coupling of the mu-CT images and the numerical models (Finite Elements and surface equation) should somewhere carefully be explained. If I understood it correctly, you have resp. do:

- time-laps mu-CT images of snow (4D)
- use a (sub-)set of 3D images as input to your numerical model
- for each chosen 3D image, pre-process and discretize (e.g., image processing, triangulation)
- determine some parameters from the geometry directly (e.g., surface curvature)
- determine other parameters from numerical modeling (e.g., growth velocity)
- compute SSA evolution using above; fit alpha to the experimental results

Yes, your description of the workflow is essentially correct. Specifically we:

1- Select a µCT time series with a given time resolution

2- Initialize the first term s^1 of the simulated SSA time series with the value deduced from the first µCT scan.

3- For each timestep t_n of the time series, we compute the SSA growth rate associated with the corresponding microstructure (using a FE simulations).

4- Use the growth rate to prolong the SSA time series from s^n to s^{n+1}.

A schematic summarizing this workflow is shown below.

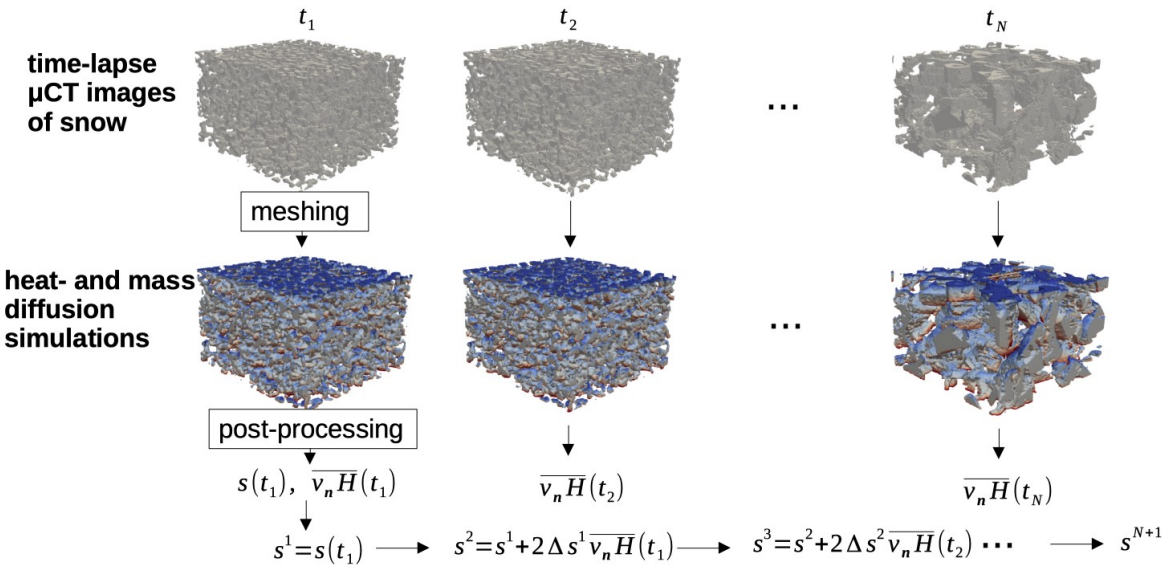

- Unclear to me are in particular:

- how many 3D images do you use for the modeling? When and how do you decide to "update" the micro-structure in your models (e.g., using a new image from the 4D series)? Or do you never do this (and always use the 1st image only)? In general, the discretization in time of the numerical model is unclear to me.

In the modeling, we use one 3D image for each timestep of a time series. As detailed above, for each timestep, we compute the evolution from s^n to s^{n+1} using the 3D image corresponding to timestep t_n. The first term s^1 of the SSA time series is initialized using the first 3D image, and the subsequent terms are computed using the growth rates deduced from the FE simulations on the 3D image of timestep t_n.

This will be specified in the text at the start of the Numerical Modeling Section **Line 140**, alongside a brief presentation of our simulation workflow:

"The end-goal of our numerical modeling is to simulate the SSA decrease of snow samples over time based on the pore-scale physics, and to compare this decrease to experimental observations. For that, we rely on time-resolved µCT images that were obtained under temperature gradient metamorphism conditions (Pinzer et al., 2012). These µCT scans provide (i) experimental data of the evolution of the SSA over time and (ii) snow-microstructures that can be used for our physical modeling. The computation of a vapor field using a FE simulation, combined with the local curvature of the snow sample, allows us to estimate $\langle v_n H \rangle$ over a given snow microstructure. With Eq. 9, this yields the evolution of the SSA during a given time interval.

As we want to reproduce the SSA evolution of entire time series, our general workflow is as follows. For a given experimental time series, we initialize the first term s^1 of the simulated SSA values using the SSA deduced from the first µCT image of the experimental time series. Then, the second simulated SSA value s^2 is computed by applying the growth rate deduced from a FE simulation performed on the first µCT image. The procedure is then repeated to compute the n^{th} term of the simulated SSA s^n using the already known value s^{n-1} and a FE simulation performed on the n-1^{th} µCT image. This workflow and its different steps are detailed in the Sections below."

We have also revised the start of Section 4.2 **Line 291** to better explain how the coarse temporal modeling is achieved:

"In the first step, we compare the temporal evolution of the SSA s between experimental data and the model using a large time step for the modeled data. For that, we downsample the experimental µCT time series to match the coarse temporal resolution and only perform FE simulations on those. Specifically, the modeled SSA values are computed with a coarse time resolution of ***Δ*** *= 48h for Series 1 (corresponding to 9 temporal points) and* ***Δ*** *~60h for Series 2 (corresponding to 15 temporal points). This reduction in numerical effort allows us to perform a sensitivity study and estimate a value for the effective condensation coefficient α that best matches the experimental data. A fixed constant α is used for each simulation. The range of alpha varies from 10^{-3} to 1 for Series 1 and from 10^{-3} to 10^{-1} for Series 2. For the comparison with these simulated data, we simply use all available experimental SSA data (acquired for a temporal resolution of 8h). The results are shown in Fig.3a,b."*

•selection of appropriate (sub)volumes from the 3D images, pre-processing and volumetric averaging: how exactly are the volumes that feed into the numerical model selected? For several parameters, volumetric averaging is performed (e.g., SSA, curvature, alpha). Is the averaging volume always the same (e.g., the entire domain)? Are we sure to have a size large enough to be representative? For the kinetic coefficient, it is very late in the paper that the concept of "effective coefficient" is introduced. Maybe the concept(s) could be introduced and justified early in an overall context.

For all simulations, we have used the largest available volume. We have performed additional simulations to determine the representativeness of the growth rate computed with different sample sizes. It is shown in the graph below. The volumes used in the article correspond to the largest ones for each sample.

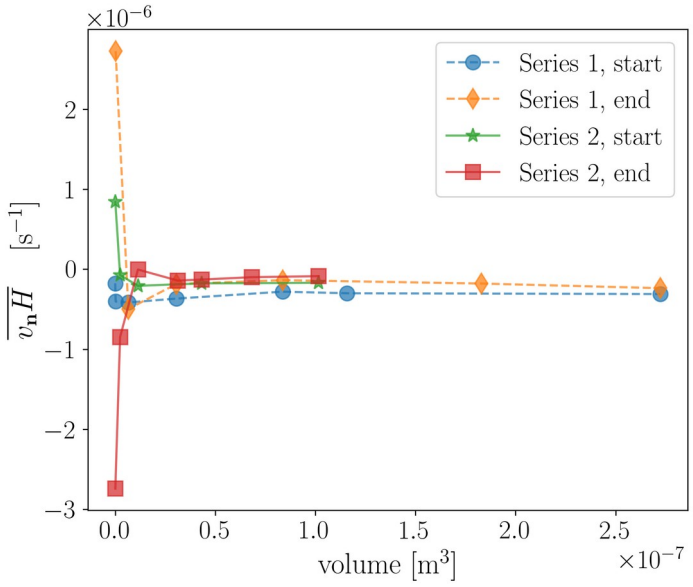

This suggests that the sample sizes used in this study are sufficient to yield representative results in terms of simulated growth rate. We will add this information **Line 179**:

"The FE meshes of this article are based on the whole available µCT images. We verified that these selected volumes were large enough to yield representative results.. By varying sub-volumes extracted from the center of µCT images at the start and the end of both series ($I(t_1)$, $I(t_{49})$, $\hat{I}(t_1)$ and $\hat{I}(t_{83})$), we found that the simulated growth rate corresponds to a representative value for

the sample sizes used in this study. This is consistent with the results of Calonne et al. (2011) for thermal conductivity, that report representativeness for sample side-lengths between 2.5 and 5mm."

Only the growth rate $\langle v_n H \rangle$ requires averaging. This averaging is performed on the whole triangulated ice-air interface of the sample. The different macroscopic quantities (SSA, growth rate, etc) are computed within the same snow volume to ensure consistency.

No averaging is performed on the condensation coefficient α, as it assumed spatially-constant in the simulations. We will specify early in the text **Line 138** that the use of a spatially-constant alpha is akin to choosing an effective value.

We will specify the use of surface average in **Lines 72** and **127** and we will clarify the definition of the growth rate in **Line 130**:

"Here the term $\overline{v_n H}$, referred to as the growth rate in this article, is the product of the local interface velocity v_n and the local mean curvature H averaged over the ice-air interface area (the surface average being indicated by an overline over the product)."

•reason for "numerical (?)" tricks like the "air padding" and iterative (2-times) solution of the energy conservation equation

Adding an artificial air-padding layer around the snow image is a numerical "trick" to obtain a surface mesh with closed outer boundaries using VTK, which is then required for meshing by CGAL. We will clarify the text about the artificial air-padding in **Line 160**:

"To this end, we employ the open-source Computational Geometry Algorithms Library (CGAL) (The CGAL Project, 2022). Specifically, we use the class Polyhedral_mesh_domain_with_features_3 that implements a tetrahedral mesh of a domain bounded by polyhedral surfaces that are preserved. The provided surfaces need to be closed and free of self-intersections. To obtain such surfaces, we extract the ice-air interface from the binary μCT data (Eq. (11) and (12)) following the procedure from (Krol and Löwe, 2018), namely by applying a Gaussian smoothing and the contour filter from the Visualization Toolkit (VTK) (Schroeder et al., 2006). However, by default this procedure applied to μCT images yields a surface that is open at the boundaries of the domain. In order to obtain closed surfaces, we added a small air-padding (three voxel-thick) around the image. This allowed us to properly define a closed outer boundary suitable for meshing. As detailed below, we provided special care to ensure that the introduction of this artificial air-padding does not perturb the simulation within the snow microstructure itself."

Solving heat equation twice is made to ensure that the presence of the air-padding does not interfere with the temperature gradient in the snow part of the mesh. We will clarify **Line 181** how we deal with air-padding in the simulation:

"For the simulation, we need to apply a given temperature gradient across the snow microstructure. However, due to the presence of artificial air-padding, directly applying the required temperature gradient across the whole FE mesh (snow plus air-padding around the image) would result in a smaller temperature gradient within the snow itself (as the air is less conducting than the snow and thus concentrates the temperature gradient). In order to obtain the proper temperature

gradient across the snow microstructure, the simulations are performed in two consecutive steps. First, the heat equation is solved over the whole FE mesh (snow plus air-padding around the image), and its result is used to estimate how a temperature gradient applied across the whole FE mesh translates into a temperature gradient within the snow microstructure itself. This allows us to compute a corrected temperature gradient to be applied across the whole FE mesh, in order to obtain the desired temperature gradient in the snow. Then, this corrected temperature gradient is used to solve the heat and mass diffusion equations with the appropriate temperature gradient across the snow microstructure. For the computation of heat and mass diffusion equations, we use the standard Elmer solvers HeatSolver and AdvectionDiffusionSolver, following Fourteau et al. (2021a).”

3. Error analysis (sections 3.4 / 4.3 / 5.3): While I do like this systematic error analysis, I find the focus very much on "time" related errors; however, I think that other errors (e.g., discretization in space) are at least equally important. These are captured and a bit discussed in section 5.3. Clearer statements – already in earlier sections – would help to better understand the strengths and weaknesses of the approach chosen.

The goal of Section of 3.4 is to propose a framework to analyze how stochastic errors in the growth rate estimation (whatever their origin) propagates and accumulates over time in the SSA. As mentioned later in the manuscript, it is meant to estimate how the temporal resolution and methodological errors combines into a given error for the SSA prediction at a give time horizon. We agree that other types of errors (such as a potential bias due to spatial discretization) are also important.

Regarding the quantification of errors, we have quantified the sensitivity of our results to the mesh resolution. This is shown in the graph below, and will be mentioned in the revised manuscript **Line 170**:

“We have estimated the sensitivity of our results to the FE mesh. We found that doubling the number of elements in the mesh impacted the growth rate by about 10%. This is small in light of the dependence of the SSA values on the condensation coefficient α investigated in this study. Moreover, the very good agreement between a FE simulation and the analytical solution for a spherical problem (see Sect. 3.6) suggests that our meshing criteria yield an appropriate mesh.”

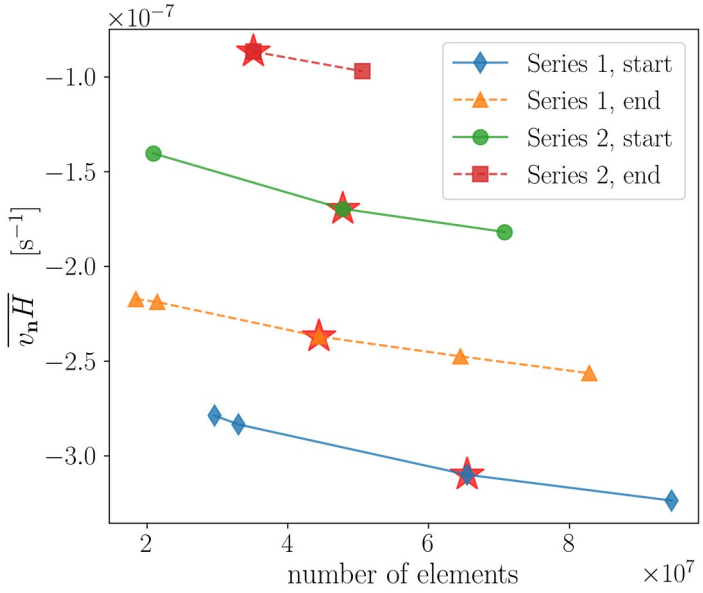

We also propose to more clearly state at the beginning of Section 3.4 that the stochastic model is meant to quantify how methodological errors accumulate over time in the SSA decrease, and the impact of the temporal resolution in this process. **Line 223**:

"While the combination of the theoretical solution of the diffusion equation and the SSA evolution is, in principle, exact, the 4D image data processing and the derived SSA are subject to experimental and processing errors. These errors could be of various origins, for instance due to uncertainties related to the estimation of the ice-air interface from the µCT scans or to errors related to the numerical FE discretization. When focusing on the temporal evolution of SSA over time, these errors will accumulate and be propagated into the modeled decrease of s(t). To analyze how these errors translates to the overall SSA decrease, and how this depends on the temporal resolution, we resort to a simple stochastic error treatment."

Line 7: suggestion: quantify the impact

We will change **Line 7** accordingly:

"[…], we quantify the impact of these […]"

Line 16: , normalized per volume. Suggestion: remove the last part of the sentence since you give many examples in the next one.

We will change **Line 16** accordingly:

"The specific surface area (SSA) of snow is the interface area between ice and air in the microstructure of porous snow, normalized per volume. The SSA is a crucial parameter for [...]"

Line 20: one key

We will change **Line 20** accordingly:

"The SSA evolution in time is one key to […]"

Line 30: well characterized uncertainties

We will change **Line 30** accordingly:

"[…] computed within well characterized uncertainties due to […]"

Line 37: maybe you could shortly explain in this paragraph why other effects are (at least here) of second order and neglected, e.g., advective transport, rigid body motion, …

We will mention in this paragraph that other processes could play a role in the evolution of SSA. See the response on Specific Remark 1.

Line 38: one key parameter…

We will change **Line 38** accordingly:

"In this picture, one key parameter driving snow metamorphism is […]"

Line 61: I think alpha also impacts numerical effort for the simpler models. Thus, suggestion: Since the choice of alpha has..., it is not surprising that…

Line 64: suggestion: at the expense of …

We will change **Line 61** accordingly:

"Since the choice of α has a significant impact on numerical effort, it is not surprising that the majority of modeling attempts exist for simplified geometries (mostly spheres) (Adams and Brown, 1982; Colbeck, 1983; Albert and McGilvary, 1992; Miller and Adams, 2009), at the expense of microstructural realism."

Line 65: detailed is somewhat misleading here (in comparison to the mu-CT models with detailed micro-structure). Suggestion to remove "detailed".

We will change **Line 65** accordingly:

"[…] are those implemented in snow cover models e.g., […]"

Line 73: it is not entirely clear to me why not both parameters could be measured experimentally (e.g., extracted from 4D mu-CT) or also both be computed by a model. Maybe you could simply say that what you propose is one possibility.

Furthermore, it seems to me that you also compute the interfacial curvature from the model.

What we meant is that when simulating the SSA evolution from a given 3D image, the computation of the curvature and interface velocity fields are fundamentally different. The first one is purely geometric and is readily accessible with the 3D image. The second is not directly given by the 3D image and requires extra knowledge about the physics at play. It is true that time-series of 3D images could be used to experimentally estimate the interface velocity, but our goal in the paper is to be able to compute how the SSA of a given microstructure evolves over time (without the need for information about the microstructure in the future).

We will specify that in the text in **Line 73**:

"While the interfacial curvature is a purely geometrical quantity that can directly be computed from a µCT image, v_n is a physical quantity that further depends on the involved physical processes."

Line 80: later, in the discussion, you (I think, correctly) say that your model works on 3D mu-CT images. I would find it useful to be clear/explicit here in the intro: do you actually use a time-series of 3D images and, for each image, calculate SSA-evolution using the model Or - vs. only use the 1st image and compute from there the SSA evolution for the whole future.

For a 3D image at time t_n, we compute the growth rate based on its microstructure and then use this growth rate to update our time series of SSA values from s^n to s^{n+1}. We will specify it at the start of the Numerical Modeling section **Line 140**, as detailed in the response to the Specific Remark 2.

Line 115: so far, alpha was called vapor attachment coefficient

We will introduce alpha in **Line 38** defining it "condensation coefficient" and mentioning that other names of alpha appear in the literature:

"In this picture, one key parameter driving snow metamorphism is the condensation coefficient α, also called attachment, kinetic or sticking coefficient (Libbrecht, 2005; Kaempfer & Plapp, 2009;

Krol & Loewe, 2016; Demange et al., 2017; K. Fourteau et al., 2021b; L. Bouvet et al., 2022) that controls the kinetics of vapor deposition and sublimation."

We will further call alpha "condensation coefficient" in abstract (**Line 8**) and throughout the text.

Line 127: hmm... you also use the mean curvature. Maybe say: this information, together with information about surface curvature, is…

We agree and therefore will change **Line 126** accordingly:

"[…] this information, together with information about surface curvature, is sufficient to […]"

Line 128: suggestion (see also comment high up, where SSA is defined): define SSA "per unit volume", remove parenthesis here.

Further down, SSA_V is introduced; maybe this could already be done at the definition high up (or there, one could at least say that the normalization can done in several ways).

minor suggestion: the "evolution equation" for SSA…

We will rewrite this subsection by first introducing both specific surface area definitions and then presenting the surface area evolution equation **Line 125**:

"In this article, we use of two SSA definitions: specific surface area per unit volume s and specific surface area per ice volume SSA_v. They are closely related through the ice volume fraction φi:

Eq. 8

We mainly work with the quantity s for the rest of the article. However, we note that the quantity SSA_v is more commonly used in the snow community (.e.g Matzl and Schneebeli, 2006), since it directly corresponds to the optical diameter.

The solution of heat and mass diffusion equations (Eq. (1)-(3)) with boundary conditions (Eq. (4)-(7)) yields […] As a result, for single grains or statistically homogeneous microstructures, the surface area evolution equation can be expressed as follows: […]"

Line 130: not entirely clear to me: do you average over the same unit volume as for the SSA? Or is it a smaller average?

The surface average is performed on the ice-air interface of a given snow volume. This strictly corresponds to the interface from which the SSA is defined.

Line 134: simplify: "Eq. (9) allows us…"

We will change **Line 134** removing the word "representation":

"Equation (9) allows us to […]"

Line 150: shorten: use mu-CT (after first having introduced the abbreviation) throughout.

Line 150: suggestion: taken instead of extracted

We will change **Line 150** accordingly:

"The µCT image data were taken from […]"

We will further change **Line 141**:

"3.1 µCT time lapse experiments"

Line 154: shouldn't voxel size be m^3 - or say "in each direction" or "cubic voxel size with side-length"

We will exchange "voxel size" with "voxel side length" in the revised manuscript **Line 154**.

Line 174: I suspect Gamma here to be the "discretized" surface - correct? This is not entirely consistent with the (general) definition of Gamma at the beginning of 2.2. The same comment holds for H. Think about, if it is worth distinguishing.

Indeed, while Gamma in the "Theoretical background" Section corresponds to the "true" ice-air interface in a snow sample, the Gamma of Line 174 corresponds to the triangulated representation. We will change Lines 173-175 accordingly:

"In addition, we computed the boundary weight on each mesh node k of the triangulated ice-air interface Γ_h

$$\omega_k = \int_{\Gamma_h} \psi_k \, d\Gamma_h \quad (13)$$

where [...]"

Line 180: suggestion: use consistent terminology (e.g., we solve the diffusion equations (1)-(3) - or alternatively, talk about Laplace eqs higher up).

We will introduce the equations in **Line 94** as (stationary) heat and mass diffusion equations mentioning that they can be called Laplace equations:

"[…], we employ the common assumption of small particle Péclet number (Libbrecht, 2005) and consider stationary heat and mass diffusion equations (i.e. Laplace equations)."

Line 181: employing the open-source...

We will change **Line 180** accordingly:

"On the tetrahedral FE mesh with preserved surface, we solve heat and mass diffusion equations (Eq. (1) - (3)) employing the open-source FE software Elmer (Malinen and Råback, 2013)."

We will further change to the consistent use throughout the whole text**.**

Line 182: these two steps are not entirely clear to me. I suggest to re-formulate it. My questions are in particular:

- why exactly is one solution of the heat equation not sufficient?

- do you really use temperature gradients as boundary conditions (i.e., flux?) and not Dirichlet temperature b.c.'s?

- is the issue the "vertial" boundary, i.e., the air gap or the boundary condition at the top and bottom?

Due to the presence of artificial air-padding, solving the heat equation once on the given FE mesh (snow image plus air-padding around the image) would result in a smaller temperature gradient

within the snow itself. We aim to obtain a correct temperature gradient within the snow structure (the same as in the experiment). To achieve this, we solve the heat equation on the FE mesh twice: the first one tells us how a gradient over the entire domain translates into the snow itself, and the second uses a corrected gradient to match the experimental gradient in the snow itself. We impose Dirichlet boundary conditions on the top and bottom of the FE mesh to apply the macroscopic temperature gradient. Note that we do not impose a microscopic gradient at the boundaries (which would be a Neumann boundary condition).

Following our response to Specific Remark 2, we will reformulate the manuscript **Line 181** to better explain these two steps.

Line 187: use consistent terminology throughout the paper: heat equation vs. diffusion equation, vs. heat diffusion equation (and similar with vapor)

We will change to the consistent use of heat and mass diffusion equations as stated in response to the comment to Line 180.

Line 207: For my clarification: is Calculate Loads simply providing the flux through an interface? If so, maybe simply say so. And, if you like, add: this can be interpreted as deposition and sublimation fluxes. I am not sure if the simulation does provide directly deposition and sublimation information.

The Elmer function Calculate Loads provides the flux at the interface nodes, expressed in kg/s. It then needs to be converted in surface flux expressed in ks/m^2/s. We will change **Line 206** accordingly:

"Finally, the required local interface velocity v_n is computed using the vapor flux deduced from the FE simulation. For this, we use the Calculate Loads option of Elmer that provides the vapor flux f_k (expressed in kg s^{-1}) at each node k of the ice-air interface. Dividing by the associated boundary weight Ω_k yields the corresponding deposition/sublimation flux (expressed in kg m^{-2} s^{-1}) over the ice-air interface."

Line 218: this sentence needs revision (no sense)

We will modify the paragraph for clarity **Line 216**:

"For that, we use the VTK package and first cut off the small air padding on the sides using vtkClipDataSet. Then, the triangulated ice-air interface is extracted. The local interface velocity v_n is directly taken from the FE simulation using Eq.(17) . For the local curvature H, we employ the image analysis derived in Krol and Loewe (2018), based on the shape operator, as explained in Section 3.2. Finally, the surface integration for the average in $\langle v_n H(t_n) \rangle$ takes into account the variable element size of the triangular mesh of the ice-air interface."

Line 222: During a 1st read, I had the impression that the error discussion focusses on discretization errors in time.

I would find it useful to clearly state the role of the variance sigma (maybe after having said "of unknown origin") and how it can include dicretization in space or smoothing related errors. Maybe even say already here how one may estimate sigma.

We will specify in the text that these errors could be of whatever origin, for instance due to the variability between the actual ice-air interface, and the reconstructed surface through µCT. **Line 223**:

"While the combination of the theoretical solution of the diffusion equation and the SSA evolution is, in principle, exact, the 4D image data processing and the derived SSA are subject to experimental and processing errors. These errors could be of various origins, for instance due to uncertainties related to the estimation of the ice-air interface from the µCT scans or to errors related to the numerical FE discretization. When focusing on the temporal evolution of SSA over time, these errors will accumulate and be propagated into the modeled decrease of s(t). To analyze how these errors translates to the overall SSA decrease, and how this depends on the temporal resolution, we resort to a simple stochastic error treatment."

Line 223: equations (heat and mass)

We will change to the consistent use of heat and mass diffusion equations as stated in response to the comment to Line 180.

Line 225: assess (instead of address)?

We will change **Line 225** accordingly:

"[…] error treatment to assess the impact of these errors."

Line 227: is there a reason to use t' here and not tau anymore? If not, I suggest to unify the notation

There is no specific reason for using t'. We will exchange t' with τ in **Eqs. (19), (20), (22) and Lines 228 and 231**. We will further correct **Eq. (21)** using τ for all terms in the equation:

"$r(\tau) = r^{true}(\tau) + \delta r(\tau)$"

Line 228: do we really want to introduced "decay rate"? is it not rather "rate of evolution"

We will change **Lines 72, 130, 134, 216, 228, 231, 363 and 442** determining v_nH as "growth rate" consistently throughout the text.

Line 233: its rather "computations" than "measurements" that are affected, I think

Indeed. We will change **Line 233** accordingly:

"[…], which affects the computations at each time step."

Line 254: should this be "and" and not "as" (?)

We will clarify the sentence **Line 253**:

"We set up a complex numerical workflow that starts from a voxel image, computes the interface velocity v_n from a FE simulation, and eventually yields the growth rate $\langle v_nH \rangle$ after surface integration."

Line 257: should we say that it is an isothermal situation?

The vapor problem between the outer and inner shells is actually temperature-independent, rather than isothermal. There is no need for a temperature field in this case. We will revise the paragraph and explain that the problem is temperature-independent **Line 255**:

"To this end, we employ the classical situation of the Laplace equation in a spherical shell for the vapor concentration $\rho_v(r)$ with radial coordinate r around a spherical particle with radius R with fixed vapor concentration ρ_∞ applied at the outer shell at distance R_∞. A Robin boundary condition (Eq. (15)) is applied at the inner surface of the sphere, under the form $Dv\, n \cdot \nabla\rho_v = \alpha\, v_{kin}[\rho_v - \rho_{v,s}]$, with $\rho_{v,s}$ a constant value smaller than ρ_∞. Note that this problem is temperature-independent and is fully determined by the radius of the shells, and the values ρ_∞ and $\rho_{v,s}$ at the boundaries."

Figure 1. b) would we not expect v_n to be either positive or negative everywhere? i.e., why is the scale going from negative to positive values?

From a physical point of view, we expect the vapor field to deposit on the inner sphere and water vapor to be added from the outer sphere to maintain the mass balance. In terms of interface velocity v_n, it is positive on the inner sphere (vapor deposition) and negative on the outer sphere (vapor sublimation). We will expand the **caption of Figure 1** specifying that there is sublimation and deposition:

"Figure 1. [...] b) Clip of the outer and inner spherical shells with visible elements colored by the interface velocity v_n (sublimation in blue, deposition in red). [...]"

We will also extent the text **Line 270** to better explain what Fig. 1b illustrates:

"*After solving the vapor equation, with appropriate boundary conditions, we obtain the interface velocity v_n, shown in Fig.1b. As expected, we observe a positive velocity on the inner shell, corresponding to vapor deposition, and a negative velocity on the outer shell, corresponding to sublimation.*"

Line 287: please introduce ancronymes when first used.

We will change **Lines 286-287** introducing the acronym:

"[...] showing the best root mean square error (RMSE) agreement [...]"

We will further change **caption of Figure 1c** and **Line 303** using only the acronym.

Line 296: does this mean that you use e.g., the 1st image to compute SSA evolution form time 0 to time 48, then the image from time 48 for the next 48h, and so on? See also my remark in the intro-section. I would find it helpful to be more clear / explicit, either above or here in the numerics section.

Yes it is exactly that. We compute the growth rate at a given time t_n using the corresponding microstructure and apply it to the SSA to compute its value at time t_{n+1}. We will clarify this in the text, following our response to the Specific Remark 2.

Figure 4: a color scheme that also works for people with color deficiency would be appreciated. Alternatively, use different "dots" or line-styles

We will improve readability of **Figure 4** by changing a color and using dashed lines:

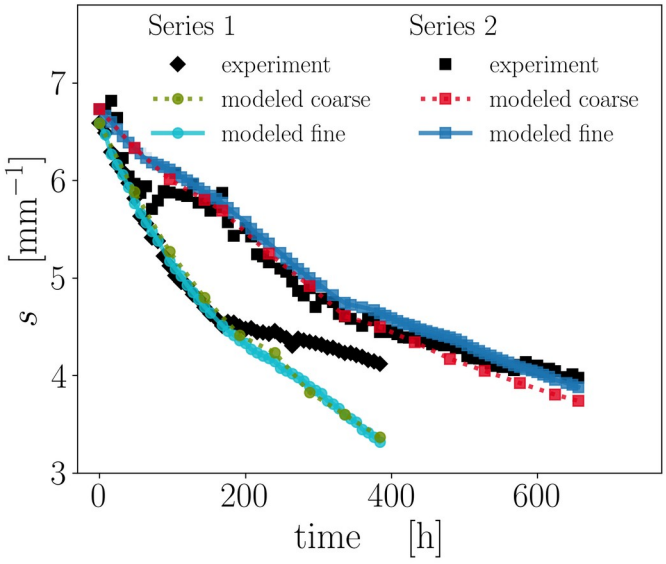

Line 308: lower (instead of deeper)

We will change **Line 308** accordingly:

"[…] for Series 2 is lower despite higher data scattering."

Line 309: is it really only temporal resolution? Is one of the values not that, when using the variance sigma, you also get an estimate of other errors?

Indeed, the stochastic model not only incorporates the temporal resolution but also the level of methodological errors. The resulting error on the SSA is the interplay of both. However, the Section mainly focuses on how varying the temporal resolution (while assuming a constant level of methodological errors) impact the modeled SSA decrease. Therefore, we would prefer to keep the title of the Section as such.

It is true that once the stochastic model is adjusted to the simulated data, we obtain a variance that *in principle* characterizes the level of stochastic methodological errors. However, before further interpreting this adjusted variance value, it would likely be beneficial to quantify the robustness of the method and to ensure that this adjusted value is indeed indicative of the overall methodological error in the simulation workflow. This is an interesting prospect for future work.

Line 310: sentence needs revision ("refined down the time interval" does not make sense)

We will change **Line 310** accordingly:

"[…] we performed simulations with a time step refined down to the time interval between […]."

Line 321: on the one hand

We will change **Line 321** accordingly:

"On the one hand, this […]"

Line 367: suggestion: "nevertheless" instead of "as a result of the numerical effort"

We will change **Line 367** accordingly:

“Nevertheless, we were able to […]”

Line 408: Indeed, I think it is a remarkable result that a somehow volumetrically averaged kinetic coefficient seems to be sufficient to explain SSA evolution. The message is here, but not very "pointy".

We will draw attention to this result by adding the following sentence to **Line 405**:

“It is quite remarkable that despite variations of the condensation coefficient at the micro-scale, their collective behavior can be appropriately described through the use of a single α value. Indeed, in principle, the assumption of a constant α [...]”

Line 420: how come the volume for the simulation impacts the experimental parameters? Can this be reformulated?

If the volume are quite close or smaller than the REV size, one could observe fluctuations in the SSA values that are due to changes in the observed Region Of Interest rather than variations due to actual evolution of the macroscopic SSA. This will be reformulated in the text **Line 418**:

“Second, the volume of interest considered here for the simulations is relatively small, in particular for Series 2. This might lead to some non-representativeness issues and fluctuations in the measured SSA. This could explain the noisy nature of the experimental parameter curves.”

Line 425: yes! I think, you should not entitle section 3 as "temporal" only and have the discussion along the line of this nice summary.

Following the Specific Remark 3, we will mention earlier in the manuscript **Line 223** that the stochastic model incorporates the interplay between temporal resolution and methodological uncertainties.

Line 434: I am not sure that non-convergence of the solver is linked to this simplification. I would keep the two discussions separate. You could e.g., justify (higher up, where it is first said) to neglect latend heat for simplicity with the argument to increase numerical stability. Then, in a separate paragraph under 5.4. say that numerical improvements might help to increase numerical convergence.

This simplification is a trade-off between numerical simplicity and physical realism. It helps the convergence of the solver, as the numerical problems to be solved are smaller and less complex, but remove a potentially important physical process.

We will explain early in the revised manuscript why latent heat is neglected **Line 108**:

“As by Krol and Löwe (2016), the latent heat during the sublimation and deposition is neglected for reduced model complexity.”

We will clarify why this simplification helps convergence, but that despite it there are still converge issues, and propose so remedy for it **Line 432**:

“This leads to a slightly simpler numerical situation where heat and vapor are coupled only one way, and the heat diffusion equation can be solved in advance. This strategy reduces the numerical cost of the method and facilitate the convergence of iterative solver used in the FE software. Despite this simplification, we still observe that the vapor solver had issues to converge for a few microstructures, which explains a few missing points in the modeled time series (e.g., Fig. 4. The convergence of the FE simulations depends on the employed mesh and on the value of α. It could be facilitated by improving the mesh quality or increasing the maximum number of iterations.”

Line 436: It seems not correct that latent heat can contribute to mass fluxes. It might possibly impact them. Please reformulate.

We will rephrase the sentence in **Line 435**:

“While this one-way coupling assumption eases the numerics, it was previously shown Fourteau et al. (2021) that for low density or fast kinetics, latent heat significantly contributes to the heat fluxes in snow and may thus likewise impact the volume averaged rate term $v_n H$.”

Line 446: I think this such a central result / conclusion that it is worth cross-checking consistency with terminology and already higher up in the document introduce the "effective kinetic coefficient", I think it is to be understood as a volumetric average.

We will introduce the notion of an “effective condensation coefficient” early in the revised manuscript in Sect. 2, **Line 123**:

“Although α is known to depend on temperature, supersaturation, crystallographic orientation and to vary on different parts of the ice-air interface (Libbrecht ,2005), we rely on the simplifying assumption of a single and constant \alpha value. It should thus rather be understood as an effective condensation coefficient.”

ADDITIONAL REFERENCES:

Demange, G., Zapolsky, H., Patte, R., and Brunel, M.: A phase field model for snow crystal growth in three dimensions, npj Computational Materials, 3, 1–7, 2017.

Ebner, P. P., Schneebeli, M., and Steinfeld, A.: Metamorphism during temperature gradient with undersaturated advective airflow in a snow sample, The Cryosphere, 10, 791–797, https://doi.org/10.5194/tc-10-791-2016, 2016.

Schleef, S., Löwe, H., and Schneebeli, M.: Influence of stress, temperature and crystal morphology on isothermal densification and specific surface area decrease of new snow, The Cryosphere, 8, 1825–1838, https://doi.org/10.5194/tc-8-1825-2014, 2014.

A rigorous approach to the specific surface area evolution in snow during temperature gradient metamorphism

Anna Braun[1,2], Kévin Fourteau[1], and Henning Löwe[1]

[1]Group Snow Physics, Research Unit Snow and Atmosphere, WSL Institute for Snow and Avalanche Research SLF, 7260 Davos Dorf, Switzerland
[2]Laboratory of Cryospheric Sciences, School of Architecture, Civil and Environmental Engineering, Ecole Polytechnique Federale de Lausanne, 1015 Lausanne, Switzerland

Correspondence: Henning Löwe (loewe@slf.ch)

Abstract. Despite being one of the most fundamental microstructural parameters of snow, the specific surface area (SSA) dynamics during temperature gradient metamorphism (TGM) have so far been addressed only within empirical modeling. To surpass this limitation, we propose a rigorous modeling of SSA dynamics using an exact equation for the temporal evolution of the surface area, fed by pore-scale finite element simulations of the water vapor field coupled with the temperature field on X-ray computed-tomography images. The proposed methodology derives from physics' first principles and thus does not rely on any empirical parameter. Since the calculated evolution of the SSA is highly sensitive to fluctuations in the experimental data, we ~~address~~ quantify the impact of these fluctuations within a stochastic error model. In our simulations, the only poorly constrained physical parameter is the ~~vapor attachment~~ condensation coefficient α~~onto ice~~. We address this problem by simulating the SSA evolution for a wide range of α and estimate optimal values by minimizing the differences between simulations and experiments. This methodology suggests that α lies in the intermediate range $10^{-3} < \alpha < 10^{-1}$ and slightly varies between experiments. Also, our results suggest a transition of the value of α in one TGM experiment, which can be explained by a transition in the underlying surface morphology. Overall, we are able to reproduce very subtle variations in the SSA evolution with correlations of $R^2 = 0.95$ and 0.99, respectively, for the two considered TGM time series. Finally, our work highlights the necessity of including kinetics effects and of using realistic microstructures to comprehend the evolution of SSA during TGM.

1 Introduction

The specific surface area (SSA) of snow is the interface area between ice and air in the microstructure of porous snow~~that determines many structural and physical properties of the snow cover~~, normalized per volume. The SSA is a crucial parameter for the optical albedo of snow (Dumont et al., 2014), fluid permeability (Zermatten et al., 2014), avalanche prediction (Schweizer et al., 2003), microwave remote sensing (Picard et al., 2022), or chemical exchange with the atmosphere (Hanot and Dominé, 1999). The SSA evolution in time is ~~the~~ one key to quantifying metamorphism (Legagneux et al., 2004; Domine et al., 2006; Pinzer et al., 2012; Wang and Baker, 2014; Harris Stuart et al., 2023) and needs to be faithfully parameterized in snow cover models to capture the evolution of physical properties. Temperature gradient metamorphism (TGM) is by far the

most important type of metamorphism in dry, natural snow covers (Schneebeli and Sokratov, 2004; Legagneux et al., 2004), since gradient-free (i.e., isothermal) conditions exist at most in deep polar firn. However, a detailed physical understanding of the SSA evolution under TGM is still lacking.

Detailed experimental data on TGM can be conveniently acquired nowadays through X-ray micro-computed tomography (μCT). Imaging of snow samples with μCT was developed over the last two decades (Coleou et al., 2001; Flin et al., 2004; Schneebeli and Sokratov, 2004; Schleef and Loewe, 2013) and provides 3D insight into the microstructure that is otherwise invisible to the naked eye. In contrast to many destructive snow measurement methods, μCT preserves the structure of the snow. Since the entire snow microstructure is available, any parameter of interest, especially SSA, can be computed within ~~established~~ well characterized uncertainties due to reconstruction and image analysis (Hagenmuller et al., 2016). By using instrumented sample holders to constrain temperatures and temperature gradients, in-situ time-lapse observations of the microstructure during TGM are obtained (Kaempfer et al., 2005; Pinzer et al., 2012; Calonne et al., 2014a; Hammonds et al., 2015; Wiese and Schneebeli, 2017; Li and Baker, 2022). While many SSA evolution curves originated from these studies, none of them has been convincingly reproduced from a physical model.

Physical models of snow metamorphism must comply with the ice crystal growth dynamics at the pore scale (Krol and Löwe, 2016), which ~~comprises vapor and heat~~ includes heat and mass diffusion, accommodated by attachment kinetics controlling the deposition and sublimation of water molecules onto the ice lattice (Colbeck, 1983; Libbrecht, 2005). ~~The key parameter in this picture is the vapor attachment~~ Secondary effects on the temporal SSA evolution might be expected from other processes like mechanical deformation (Wang and Baker, 2013; Schleef et al., 2014), advection of air in the porosity (Ebner et al., 2016; Jafari et al., 2022). In this picture, one key parameter driving snow metamorphism is the condensation coefficient α, also called attachment, kinetic or sticking coefficient (Libbrecht, 2005; Kaempfer and Plapp, 2009; Krol and Löwe, 2016; Deman that controls the kinetics of vapor deposition and sublimation. The ~~kinetic parameter~~ condensation coefficient is applicable at the micro-meter scale of ambient diffusion processes and thereby subsumes the underlying nano-scale kinetics resulting from the molecular dynamics on the surface of the ice crystal lattice (Saito, 1996). Many measurement and modeling attempts carefully characterize α for ice crystals (Libbrecht, 2005; Hobbs, 2010; Barrett et al., 2012; Libbrecht and Rickerby, 2013; Pokrifka et al., 2020). Nevertheless, α is experimentally challenging to constrain even for isolated crystal growth. One reason is the fundamental, experimental difficulty of inverting growth data as soon as diffusion is involved (Libbrecht, 2005). The other reason is that α depends on numerous effects such as temperature, supersaturation, and crystallographic orientation (Saito, 1996; Libbrecht, 2005). The large variations between basal and prismatic surface kinetics are, for example, the key to snow crystal morphology (Barrett et al., 2012). The situation is even more complicated in the snow cover where many different surface orientations exist simultaneously (Granger et al., 2021). Therefore, the kinetics is more difficult to assess in snow, and only a few studies exist constraining α from the comparison of μCT-based simulations with experiments (Bouvet et al., 2022; Fourteau et al., 2021a). Thus, α constitutes the great unknown in snow metamorphism as commonly stressed in TGM models (Miller and Adams, 2009; Kaempfer and Plapp, 2009; Calonne et al., 2014b).

Model attempts characterizing TGM can be classified by their treatment of attachment kinetics and whether the microstructure is taken from μCT or geometrically idealized. Using μCT images, (Flin and Brzoska, 2008) calculated deposition fluxes

in the absence of kinetics under the assumption of local equilibrium at the interface (diffusion-limited growth). A similar approximation was used in (Krol and Löwe, 2016) to relate the temperature gradient driven deposition fluxes to measured, local ~~growth~~ interface velocities. The latter can be considered as a generalization of the (diffusion-limited) air bubble migration under a temperature gradient in ice (Shreve, 1967) to complex geometries. However, the assumption of purely diffusion-limited growth was already questioned (Krol and Löwe, 2018) due to contradictions with the measured SSA evolution. The μCT-based theoretical homogenization (Calonne et al., 2014b), in contrast, applies to the slow kinetics (i.e., kinetics-limited) regime. The intermediate regime from diffusion to kinetics vapor transport under a temperature gradient was numerically analyzed in (Fourteau et al., 2021a), where the latter approach is physically similar to the phase field model (Kaempfer and Plapp, 2009). ~~Common to all μCT-based approaches is that~~ Since the choice of α has a significant impact on numerical effort~~. It is therefore~~, it is not surprising that the majority of modeling attempts exist for simplified geometries (mostly spheres) (Adams and Brown, 1982; Colbeck, 1983; Albert and McGilvary, 1992; Miller and Adams, 2009), at the ~~downside~~ expense of microstructural realism. The most widely used models for predicting the SSA evolution under TGM are those implemented in ~~detailed~~ snow cover models e.g., (Flanner and Zender, 2006). Like other simplified models, (Flanner and Zender, 2006) neglect kinetics and employ diffusion-limited growth for distribution of spherical particles. Due to the involved empirical parameters (mean sphere radius and spacing), which prevent an unambiguous mapping onto arbitrary microstructures, validating these models through μCT laboratory experiments would remain inconclusive.

In principle, no empiricism is required, and the SSA evolution for arbitrary 3D microstructure can be computed exactly (Krol and Löwe, 2018), as long as the required parameters are supplied. The surface area equation is rigorously formulated ~~in terms of a rate term~~ on the basis of a growth rate that can be computed from the interfacial curvature and the interface ~~growth~~ velocity $v_\mathbf{n}$ after ~~volume~~ surface averaging. While the ~~first is a geometrical quantity, the second must~~ interfacial curvature is a purely geometrical quantity that can directly be computed from a ~~physical model. Any~~ μCT image, $v_\mathbf{n}$ is a physical quantity that further depends on the involved physical processes. In this framework, any model that predicts $v_\mathbf{n}$ as the result of 3D heat and mass diffusion with interface kinetics could be employed here, either phase field models (Kaempfer and Plapp, 2009) or diffusion models (Fourteau et al., 2021b). Both are equivalent in view of the involved physics and only differ in their representation of the interface. This route to the SSA evolution in TGM is rigorous (apart from numerical approximations) but has never been pursued before. Advancing on this route is the aim of the present work. To this end, we combine a finite element (FE) solution of the pore-scale ~~vapor and heat~~ heat and mass diffusion equations following (Fourteau et al., 2021b) with the exact surface area equation from (Krol and Löwe, 2018) in order to reproduce the SSA evolution during TGM from the four-dimensional (4D) μCT image data from (Pinzer et al., 2012).

The manuscript is organized as follows. The theoretical background for pore-scale diffusion and the SSA is presented in Sect. 2. In Sect. 3, we describe the numerical procedures (meshing, FE solution, image processing), a simple stochastic error analysis, and the validation of our numerical workflow against an analytical solution. The simulations for the TGM time series are shown in Sect. 4 and discussed in Sect. 5.

2 Theoretical background

2.1 Heat and vapor transfer at the pore scale

For an arbitrary snow structure, morphological changes during metamorphism are predominantly driven by the coupled diffusion of heat and mass together with ice-air interface ~~motion~~ evolution due to deposition and sublimation of vapor. In the following, we closely follow the descriptions by (Kaempfer and Plapp, 2009; Calonne et al., 2014b; Krol and Löwe, 2016; Fourteau et al., 2021a). We consider a representative snow volume at the micro-scale consisting of ice and air and denote the sub-domains occupied by the ~~solid~~ ice and air phase by Ω_i and Ω_a, respectively. In the following, subscripts i and a denote quantities which are defined in the respective domains Ω_i and Ω_a. Due to the separation of time scales between ~~the diffusion of~~ heat and mass diffusion in the pores and the ~~motion~~ evolution of the interface~~due to crystal growth~~, we employ the common assumption of small particle ~~Peclet numbers~~ Péclet number (Libbrecht, 2005) and consider stationary ~~diffusion equations for~~ heat and mass ~~. Accordingly, the~~ diffusion equations (i.e., Laplace equations). Furthermore, we neglect the influence of mechanical deformation, as usually done in pore-scale metamorphism models (e.g., (Calonne et al., 2014b; Krol and Löwe, 2016)). We also neglect the potential presence of convection and air advection in the pore space. These assumptions are consistent with the experimental data used in this article, obtained under controlled laboratory conditions (Pinzer et al., 2012). They are also good candidates in terms of minimum-required complexity to model SSA evolution from pore-scale physics. The partial density of water vapor in air ρ_v and the ice and air temperatures T_i and T_a, respectively, are governed by

$$D_v \nabla^2 \rho_v = 0 \qquad \text{in } \Omega_a \tag{1}$$

$$\kappa_a \nabla^2 T_a = 0 \qquad \text{in } \Omega_a \tag{2}$$

$$\kappa_i \nabla^2 T_i = 0 \qquad \text{in } \Omega_i \tag{3}$$

where D_v is the vapor diffusion constant in air, κ_i and κ_a are the thermal diffusivities of ice and air, respectively.

The heat and mass diffusion equations are coupled via boundary conditions on the ice-air interface Γ. The mass conservation at the ice-air interface is linked to the water vapor concentration by a Stefan-type condition

$$(\rho_i - \rho_v)\, v_{\mathbf{n}} \;=\; D_v\, \mathbf{n} \cdot \nabla \rho_v \qquad \text{on } \Gamma \tag{4}$$

where ρ_i denotes the ice density and $\mathbf{n}$ the unit normal vector field on Γ which is oriented into the pore space Ω_a and $v_{\mathbf{n}}$ is the ~~growth~~ interface velocity on Γ in the direction of $\mathbf{n}$. The velocity $v_{\mathbf{n}}$ is therefore positive for deposition and negative for sublimation.

The conservation of energy requires the continuity of temperature and heat flux on the ice-air interface according to

$$T_i \;=\; T_a \qquad \text{on } \Gamma \tag{5}$$

$$\kappa_i\, \mathbf{n} \cdot \nabla T_i \;=\; \kappa_a\, \mathbf{n} \cdot \nabla T_a \qquad \text{on } \Gamma \tag{6}$$

As ~~in~~ by (Krol and Löwe, 2016), the latent heat during the sublimation and deposition is neglected for reduced model complexity. Since mass and energy conservation involves the unknown interface velocity $v_{\mathbf{n}}$, the internal boundary condi-

tions must be completed by a constitutive law that characterizes $v_\mathbf{n}$ during crystal growth. Here, we employ the Hertz-Knudsen law (Libbrecht, 2005; Kaempfer and Plapp, 2009; Fourteau et al., 2021a), which includes the impact of interfacial curvature on the equilibrium vapor concentration (Gibbs-Thomson effect) according to

$$\rho_v = \rho_{v,s}(T)(1 + d_0\, H) + \frac{\rho_i}{\alpha\, v_{\text{kin}}} v_\mathbf{n} \qquad \text{on } \Gamma \tag{7}$$

The equilibrium (or saturation) vapor concentration on a flat surface at temperature T is denoted by $\rho_{v,s}(T)$, the capillary length by d_0, the mean curvature by H, the condensation coefficient by α and the kinetic velocity by v_{kin}. The capillary length is related to $d_0 = \gamma\, a^3/(k_B\, T)$, where γ is the interfacial free energy, a is the mean intermolecular spacing of water molecules in ice and k_B is the Boltzmann constant. The kinetic velocity is defined here as $v_{\text{kin}} = \sqrt{k_B\, T/(2\,\pi\, m)}$ with the mass of water molecule m. This definition follows (Fourteau et al., 2021a) and thus differs from the definition in (Libbrecht, 2005). In the Hertz-Knudsen equation, the ~~kinetic~~ condensation coefficient α ~~has the meaning of a sticking probability of water molecules impinging onto the surface~~ is defined as the probability of a water molecule sticking to a surface after impinging on it. Therefore, values in the range $[0, 1]$ are commonly desired, where $\alpha \to 0$ corresponds to slow surface kinetics and for $\alpha \approx 1$ the diffusion dominated regime will be attained (Libbrecht, 2005; Fourteau et al., 2021a). Mathematically the equation remains well-defined also for $\alpha > 1$, which may be physically interpreted as deviations from the local constitutive behavior ~~(7)~~ (Eq. (7)) due to non-local surface processes (Libbrecht, 2005). Although α is known to depend on temperature, supersaturation, crystallographic orientation and vary on different parts of the ice-air interface (Libbrecht, 2005), we rely on the simplifying assumption of a single and constant α value. It should thus rather be understood as an *effective* condensation coefficient.

2.2 Evolution of SSA

In this article, we use of two SSA definitions: specific surface area per unit volume s and specific surface area per ice volume SSA_V. They are closely related through the ice volume fraction ϕ_i:

$$SSA_V = \frac{s}{\phi_i} \tag{8}$$

We mainly work with the quantity s for the rest of the article. However, we note that the quantity SSA_V is more commonly used in the snow community (e.g., Matzl and Schneebeli, 2006), since it directly corresponds to the optical diameter.

The solution of the ~~diffusion system~~ heat and mass diffusion equations (Eq. (1)-(3)) with boundary conditions (Eq. (4)-(7)) yields the spatially varying ~~growth~~ interface velocity $v_\mathbf{n}$ at any point on the ice-air interface Γ. As shown by (Drew, 1990; Krol and Löwe, 2018), this information, together with information about surface curvature, is sufficient to calculate the evolution of the SSA rigorously via ~~volume~~ surface averaging. As a result, for single grains or statistically homogeneous microstructures, the ~~equation for specific surface area (per unit volume) s~~ surface area evolution equation can be expressed as follows:

$$\dot{s} = 2\, s\, \overline{v_\mathbf{n} H} \tag{9}$$

Here the ~~rate~~ term $\overline{v_\mathbf{n} H}$, referred to as the growth rate in this article, is the product of the local interface velocity $v_\mathbf{n}$ and the local mean curvature H averaged over the ice-air interface area (the surface average being indicated by an overline over the

product). Equation (9) is a linear homogeneous first-order ordinary differential equation and can be formally solved in closed form by separation of variables yielding

$$s(t) = s(0) \exp\left(2 \int_0^t \overline{v_{\mathbf{n}} H}(\tau) d\tau\right) \tag{10}$$

~~The representation Eq.~~ Equation (10) allows us to compute the SSA evolution from the ~~rate term~~ growth rate $\overline{v_{\mathbf{n}} H}$ which must be computed from the solution of the 3D diffusion problem. This link between the SSA evolution and ~~the~~ heat and mass diffusion equations is rigorous. ~~The closely related specific surface area (per ice volume) SSA_V can then be computed as~~

$$SSA_V = \frac{s}{\phi_i}$$

~~in terms of the ice volume fraction ϕ_i. The quantity SSA_V is more commonly used in the snow community (e.g., Matzl and Schneebeli, 200 since it directly defines the optical diameter.~~

3 Numerical modeling

3.1 ~~Micro tomography time lapse experiments~~

The end-goal of our numerical modeling is to simulate the SSA decrease of snow samples over time based on the pore-scale physics, and to compare this decrease to experimental observations. For that, we rely on time-resolved μCT images that were obtained under TGM conditions (Pinzer et al., 2012). These μCT scans provide (i) experimental data of the evolution of the SSA over time and (ii) snow-microstructures that can be used for our physical modeling. The computation of a vapor field using a FE simulation, combined with the local curvature of the snow sample, allows us to estimate $\overline{v_{\mathbf{n}} H}$ over a given snow microstructure. With Eq. 9, this yields the evolution of the SSA during a given time interval.

As we want to reproduce the SSA evolution of entire time series, our general workflow is as follows. For a given experimental time series, we initialize the first term s^1 of the simulated SSA values using the SSA deduced from the first μCT image of the experimental time series. Then, the second simulated SSA value s^2 is computed by applying the growth rate deduced from a FE simulation performed on the first μCT image. The procedure is then repeated to compute the n^{th} term of the simulated SSA s^n using the already known value s^{n-1} and a FE simulation performed on the $n-1^{\text{th}}$ μCT image. This workflow and its different steps are detailed in the Sections below.

3.1 μCT time lapse experiments

The numerical simulations were conducted on 4D image data of two TGM experiments (Series 1 and 2), which were previously acquired and already analyzed in (Pinzer et al., 2012) and (Krol and Löwe, 2016). In the experiments, a constant temperature gradient was applied by adjusting a snow samples's bottom and top temperature in an instrumented tomography sample holder, known as Snowbreeder (Pinzer and Schneebeli, 2009a). Series 1 lasted 384 h~~and is shorter than~~, while Series 2 ~~, which~~ lasted

665 h. The mean temperature T of the sample and the temperature gradient ∇T are similar for the both series: T = -8.1 °C, $\nabla T = 47$ Km^{-1} for Series 1 and T = -7.6 °C, $\nabla T = 55$ Km^{-1} for Series 2. Both time series start from rounded grains with slightly different initial values of SSA and volumetric density, namely $SSA_V(t=0) = 20$ mm^{-1}, $\phi_i(t=0) = 0.31$ for Series 1 and $SSA_V(t=0) = 24$ mm^{-1}, $\phi_i(t=0) = 0.28$ for Series 2. For further experimental details, we refer to (Pinzer et al., 2012).

The ~~X-ray micro-computed tomography~~ μCT image data were ~~extracted~~ taken from the snow sample every eight hours in time-lapse mode and segmented into binary images as described previously (Pinzer et al., 2012). These binary images are denoted by

$$I(t_n), \quad n = 1,2,\ldots,49 \qquad \text{for Series 1} \tag{11}$$

$$\tilde{I}(t_m), \quad m = 1,2,\ldots,84 \qquad \text{for Series 2} \tag{12}$$

at different time steps and are $300 \times 300 \times 196$ voxel images with voxel size length of $25 \cdot 10^{-6}$ m in Series 1 and of $18 \cdot 10^{-6}$ m in Series 2. This corresponds to samples of $7.5 \times 7.5 \times 4.9$ mm^3 for series 1 and $5.4 \times 5.4 \times 3.5$ mm^3 for series 2. Both series show the commonly observed decay of SSA (Taillandier et al., 2007; Pinzer and Schneebeli, 2009b; Calonne et al., 2014a).

3.2 FE solution of temperature and vapor fields

3.2.1 Meshing

~~An~~ The production of an appropriate mesh that discretizes the air and ice domains, preserves the ice-air interface~~and produces a reasonable volumetric division is~~ , and is fine enough to get accurate numerical solution (without overloading computational resources) is a key requirement for ~~an accurate numerical solution to the~~ our problem. To this end, we employ the open-source Computational Geometry Algorithms Library (CGAL) (The CGAL Project, 2022)~~and use the `Polyhedral_mesh_domain_with_fe` class that implements volume~~ . Specifically, we use the class `Polyhedral_mesh_domain_with_features_3` that implements a tetrahedral meshing of a domain ~~that is bounded by a polyhedral surface which is preserved . The surface needs~~ bounded by polyhedral surfaces, which are preserved during the meshing process. The provided surfaces need to be closed and free of ~~intersections~~self-intersections. To obtain such ~~a closed surface~~surfaces, we extract the ice-air interface from the binary μCT data (Eq. (11) and (12)) following the procedure from (Krol and Löwe, 2018), namely by applying a Gaussian smoothing and the contour filter from the Visualization Toolkit (VTK) (Schroeder et al., 2006). ~~The snow microstructure is then enclosed in a cubic domain, with a small air padding on the sides, defining the simulated domain's outer boundaries~~However, by default this procedure applied to μCT images yields a surface that is open at the boundaries of the domain. In order to obtain closed surfaces, we added a small air-padding (three voxel-thick) around the image. This allowed us to properly define a closed outer boundary suitable for meshing. As detailed below, we provided special care ~~so that this air padding~~ to ensure that the introduction of this artificial air-padding does not perturb the simulation within the snow microstructure itself. `MeshCriteria` parameters control the meshing algorithm in CGAL: Mesh tetrahedra are regulated by the radius-edge ratio upper bound of 1.5 and circumradius upper bound of 3 voxels, and triangles in the boundary surface mesh by the lower an-

gular bound of 25° and radius upper bound of 0.75 voxels. These mesh parameters were manually fine-tuned through visual inspection. ~~An objective validation of all involved parametersis provided later.~~ We have estimated the sensitivity of our results to the mesh parameters. We found that doubling the number of elements in the mesh impacted the simulated growth rate by about 10%. This is small in light of the dependence of the SSA values on the condensation coefficient α investigated in this study. Moreover, the very good agreement between a FE simulation and the analytical solution for a spherical problem (see Sect. 3.5) suggests that our meshing criteria yield an appropriate mesh. We save the mesh in four files listing the nodes, bulk elements, boundary elements, and header information, defining a mesh in the format of the FE software Elmer (Malinen and Råback, 2013). In addition, we computed the boundary weight on each mesh node k of the triangulated ice-air interface Γ_h

$$\omega_k = \int_{\Gamma_h} \psi_k \, d\Gamma_h \tag{13}$$

where ψ_k is the basis function assigned to the node k, so that the sum of all boundary weights ω_k gives the area of the whole boundary surface. Saving boundary weights is substantial for the computation of the ~~growth~~ interface velocities as surface integrals over the solution of ~~the~~ heat and mass diffusion equations. For consistency and accuracy, employing the same integration scheme that underlies the FE solution is advantageous.

The FE meshes of this article are based on the whole available μCT images. We verified that these selected volumes were large enough to yield representative results. By varying sub-volumes extracted from the center of μCT images at the start and the end of both series ($I(t_1)$, $I(t_{49})$, $\tilde{I}(t_1)$ and $\tilde{I}(t_8 3)$), we found that the simulated growth rate corresponds to a representative value for the sample sizes used in this study. This is consistent with the results of (Calonne et al., 2011) for thermal conductivity, that report representativeness for sample side-lengths between 2.5 and 5 mm.

3.2.2 FE solution

On the tetrahedral FE mesh with preserved surface, we solve ~~Laplace equations for temperature and water vapor~~ heat and mass diffusion equations (Eq. (1) - (3)) employing open-source FE software Elmer (Malinen and Råback, 2013). For the simulation, we need to apply a given temperature gradient across the snow microstructure. However, due to the presence of artificial air-padding, directly applying the required temperature gradient across the whole FE mesh (snow plus air-padding around the image) would result in a smaller temperature gradient within the snow itself (as the air is less conducting than the snow and thus concentrates the temperature gradient). In order to ~~solve the equations with the~~ obtain the proper temperature gradient across the snow microstructure, the simulations are performed in two consecutive steps. First, the heat ~~equation over the entire domain is solved~~ diffusion equation is solved over the whole FE mesh (snow plus air-padding around the image), and its result is used to estimate how a temperature gradient applied across the whole ~~domain (snow microstructure together with the small air padding on the sides) translates into~~ FE mesh translates into a temperature gradient within the snow microstructure itself. This allows us to ~~compute a corrected~~ determine a corrected temperature gradient to be applied across the whole ~~domain to match the experimental~~ FE mesh, in order to obtain the desired temperature gradient in the snow. Then, this corrected temperature gradient is used to solve the heat and ~~water vapor diffusion are solved using the corrected~~

~~temperature gradient as boundary conditions~~mass diffusion equations with the appropriate temperature gradient across the snow microstructure. For the computation of heat and ~~vapor~~ mass diffusion equations, we use the standard Elmer solvers `HeatSolver` and `AdvectionDiffusionSolver`, following Fourteau et al. (2021a). The equations are solved with the iterative biconjugate gradient stabilized method (BiCGSTAB; Van der Vorst, 1992) with an `ILU` preconditioner, meant to facilitate the numerical solving by performing an incomplete LU factorization (Saad, 2003). The maximum number of iterations is set to 2000, and the convergence tolerance to 10^{-10} for the heat diffusion equation and 10^{-12} for the mass diffusion equation. The correct temperature gradient across the domain is applied by setting top and bottom temperatures to

$$T_{\text{top}} = T - \frac{h \cdot \nabla T}{2}, \qquad T_{\text{bottom}} = T + \frac{h \cdot \nabla T}{2}, \tag{14}$$

where T and ∇T are the experimental temperatures and temperature gradient and h is the total height of the sample.

For the vapor boundary condition, we combine the Stefan condition (Eq. (4)) by neglecting the $\rho_v v_{\mathbf{n}}$ term due to $\rho_v \ll \rho_i$, and the Gibbs-Thomson equation (Eq. (7)) to obtain a Robin boundary condition at the ice-air interface

$$D_v \, \mathbf{n} \cdot \nabla \rho_v = \alpha v_{\text{kin}} [\rho_v - \rho_{v,s}(1 + d_0 H)], \qquad v_{\text{kin}} \approx 140 \, \text{m s}^{-1}, \; d_0 \approx 10^{-9} \, \text{m} \tag{15}$$

Here, the equilibrium water vapor concentration is given by the Clausius-Clapeyron relation, corrected for the Gibbs-Thomson effect: (Fourteau et al., 2021a)

$$\rho_{v,s} = \frac{M}{RT} P_0 \exp\left(\frac{L}{R}\left(\frac{1}{T_0} - \frac{1}{T}(1 + d_0 H)\right)\right), \qquad \frac{m P_0}{R} \approx 1.32 \, \text{kg K m}^{-3}, \; \frac{L}{R} \approx 6140 \, \text{K}, \; T_0 \approx 273 \, \text{K} \tag{16}$$

where M is the molar mass of water, R is the ideal gas constant, L is the latent heat of sublimation of ice, T_0 is the reference temperature and P_0 is the saturation pressure at T_0. In contrast to (Calonne et al., 2014b; Fourteau et al., 2021a), the curvature term $d_0 H$ is not neglected. The mean curvature H on the surface mesh is obtained following (Krol and Löwe, 2018) involving the shape operator computed with the normal vector field. We compute the field of normal vectors $\mathbf{n}$ using the dedicated routine of Elmer. It was found to be more reliable than VTK computations performed on the CGAL mesh, as the latter sometimes produces areas with reversed normal vectors.

Finally, the required local interface velocity $v_{\mathbf{n}}$ is computed using the ~~deposition and sublimation fluxes provided by the FE simulations~~vapor flux deduced from the FE simulation. For this, we use the `Calculate Loads` option of Elmer that provides the ~~quantity of water vapor~~ vapor flux f_k ~~removed or injected~~ (expressed in kg s^{-1}) at each node k of the ~~air ice~~ ice-air interface. Dividing by the associated boundary weight ω_k ~~from Eq. (13) yields the~~ yields the corresponding deposition/sublimation flux ~~at~~ (expressed in kg m^{-2} s^{-1}) over the ice-air interface. Thus, the interface velocity at node k is recovered from the simulation as

$$(v_{\mathbf{n}})_k = -\frac{f_k}{\omega_k \rho_i} \tag{17}$$

3.3 Post-processing and derived SSA evolution

For a given time sequence $t_1, t_2, \ldots t_N = t$ with $t_N = N\Delta$ of available μCT images (Eqs. (11), (12)) and available FE solutions of the vapor field, the SSA is inferred from the discretized solution of Eq. (9) obtained with forward Euler method

$$s^{n+1} = s^n + 2\Delta s^n \, \overline{v_{\mathbf{n}} H}(t_n)) \tag{18}$$

where $s^n := s(t_n)$. The rates $\overline{v_{\mathbf{n}} H}(t_n)$ are calculated for each time step t_n as surface integrals from the 3D FE solution. For that, we use the VTK package and first cut off the small air padding on the sides using `vtkClipDataSet` ~~and extracted the preserved by meshing~~ . Then, the triangulated ice-air ~~interface. Thenwe employ the image analysis derived in (Krol and Löwe, 2018) , where the discretized local curvature H (identical to the input used in Eq. (15)) is calculated from the shape operator~~interface is extracted. The local interface velocity $v_{\mathbf{n}}$ is ~~deduced~~ directly taken from the FE simulation using Eq. (17). ~~The~~ For the local curvature H, we employ the image analysis derived in Krol and Löwe (2018), which is based on the shape operator, as explained in Section 3.2.2. Finally, the surface integration for the average in $\overline{v_{\mathbf{n}} H}(t_n)$ takes into account the variable element size of the triangular mesh of the ice-air interface.

3.4 Stochastic model for the discretization error

While the combination of the theoretical solution of the diffusion equation and the SSA evolution is, in principle, exact, the 4D image data processing and the derived SSA are subject to experimental and processing errors~~, which propagate~~ . These errors could be of various origins, for instance due to uncertainties related to the estimation of the ice-air interface from the μCT scans or to errors related to the numerical FE discretization. When simulating on the temporal evolution of SSA over time, these errors will accumulate and be propagated into the modeled decrease of $s(t)$. ~~We~~ To analyze how these errors translates to the overall SSA decrease, and how this depends on the temporal resolution, we resort to a simple stochastic error treatment~~to address the impact of these errors~~. To this end, we write the rigorous representation of the SSA evolution from above as

$$s^{\text{true}}(t) = s(0) \, \exp\left(2 \int_0^t dt' d\tau \, r^{\text{true}}(t'\tau) \right) \tag{19}$$

and indicate that the true decay rate ~~$r^{\text{true}}(t') = \overline{v_{\mathbf{n}} H}$~~ $r^{\text{true}}(\tau) = \overline{v_{\mathbf{n}} H}$ is in general unknown and concealed by errors. In the simplest setting, one would expect that the predicted SSA can, therefore, be written as

$$s(t) = s(0) \exp\left(2 \int_0^t dt' d\tau \, r(t'\tau) \right) \tag{20}$$

where the measured rate ~~$r(t')$~~ $r(\tau)$ differs from the true rate by a noise term via

$$r(t\tau) = r^{\text{true}}(t'\tau) + \delta r(t\tau) \tag{21}$$

Here, ~~$\delta r(t)$~~ δr is an additive noise, representing uncorrelated errors (for now of unspecified origin), which affects the ~~measurements~~ computations at each time step. This implies that, on average, the computed SSA estimates are not equal to the true value s^{true} but rather to

$$s(t) = s^{\text{true}}(t) \left\langle \exp\left(2 \int_0^t dt' d\tau \, \delta r(t'\tau) \right) \right\rangle \tag{22}$$

where $\langle \bullet \rangle$ denotes the average with respect to the additive noise. For a finite time step Δ, the discrete solution can now be written as

$$s_\Delta(t) = s^{\text{true}}(t) \left\langle \exp\left(2\Delta \sum_{i=1}^{N} \delta r(t_i) \right) \right\rangle \tag{23}$$

where the dependence on the time step Δ has been made explicit in the notation. For uncorrelated measurement errors, we assume $\delta r_i := \delta r(t_i)$ to be i.i.d. Gaussian random variables with zero mean and variance $\langle \delta r_i^2 \rangle = \sigma^2$. Since the averaged exponential in Eq. (23) is nothing but the characteristic function of δr_i, the average can be readily calculated and written as

$$s_\Delta(t) = s^{\text{true}}(t) \exp(2\Delta\sigma^2 t) \tag{24}$$

Since the truth in Eq. (24) is unknown, *absolute* errors are a priori not accessible. However, we can exploit Eq. (24) to define a *relative* error metric that quantifies the differences due to different temporal resolutions when integrating Eq. (19). To this end, we define

$$\varepsilon(\Delta, \Delta', t) := \frac{(s_\Delta(t) - s_{\Delta'}(t))^2}{s_\Delta(t)^2} \tag{25}$$

which allows us to assess the influence of using different time steps in the SSA evolution. By simplifying Eq. (25) we infer

$$\varepsilon(\Delta, \Delta', t) = [1 - \exp(2|\Delta - \Delta'|\sigma^2 t)]^2 \tag{26}$$

which relates simulated SSA differences at time t to the temporal resolution of the model and the variance of the measurement error σ.

3.5 Workflow validation: Growth of a spherical shell

We set up a complex numerical workflow that starts from a voxel image, computes the interface velocity $v_\mathbf{n}$ from a FE simulation, and eventually yields ~~a~~ the growth rate $\overline{v_\mathbf{n} H}$ ~~that is computed by image analysis as a volume average from the 3D results of the FE solution~~after surface integration. In order to validate the entire workflow, we consider a test case that can be compared to an analytical solution. To this end, we employ the classical situation of the Laplace equation in a spherical shell for the vapor concentration $\rho_v(r)$ with radial coordinate r around a spherical particle with radius R with fixed vapor concentration ρ_∞ applied at the outer shell at distance R_∞. ~~The Robin boundary conditions~~ A Robin boundary condition (Eq. (15)) ~~are~~ is applied at the inner surface of the sphere, under the form $D_v \mathbf{n} \cdot \nabla \rho_v = \alpha v_{\text{kin}} [\rho_v - \rho_{v,s}]$, with $\rho_{v,s}$ a constant value smaller than ρ_∞. Note that this problem is temperature-independent and is fully determined by the radius of the shells, and the values of ρ_∞ and $\rho_{v,s}$. In this case, the ~~growth~~ interface velocity is known analytically (e.g., (Carslaw and Jaeger, 1986)), and due to spherical symmetry, the growth rate averaged over the surface is given by the value of the solution at $r = R$, via

$$\overline{v_\mathbf{n} H} = \frac{v_\mathbf{n}}{R} = \frac{D_v}{\rho_i} \frac{\rho_\infty - \rho_{v,s}}{R\left(R - \frac{R^2}{R_\infty} + \frac{D_v}{\alpha v_{\text{kin}}}\right)} \tag{27}$$

This analytical solution is compared to the numerical solution as follows. We start from a voxel image representation of the spherical shell as illustrated by the inner sphere in Fig. 1a, where the inner radius is set to ~~$R = 21$~~ $R = 10$ voxel and

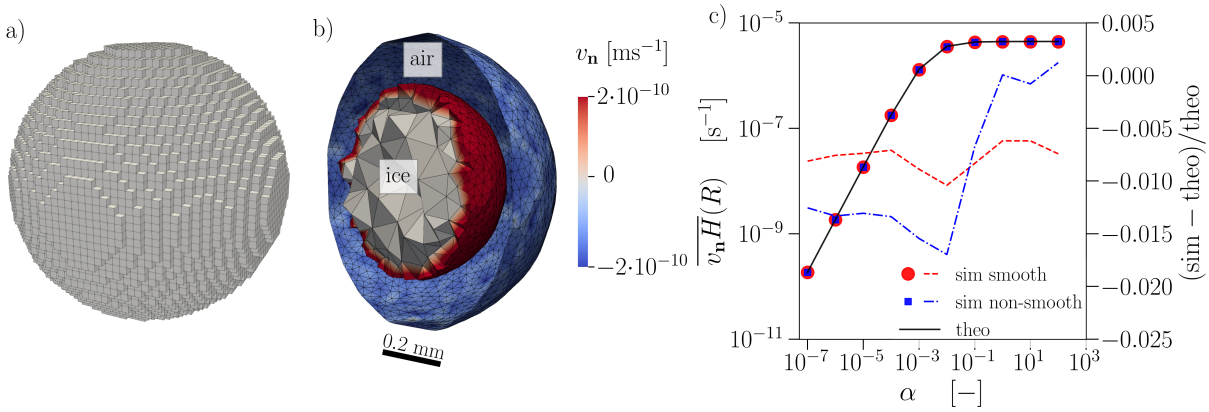

Figure 1. a) Voxeled sphere obtained from ~~the~~ a binary image and used to constrain the problem. b) Clip of the outer and inner spherical ~~shell~~ shells with visible ~~finite~~ elements colored by the ~~growth~~ interface velocity $v_\mathbf{n}$ (sublimation in blue, deposition in red). c) Comparison of the growth rate $\overline{v_\mathbf{n}H}$ on the inner radius R of theoretical (theo) and simulated (sim) solution of the spherical shell test case for different values of ~~vapor attachment~~ the condensation coefficient α. Two different surface mesh qualities with (smooth) and without (non-smooth) smoothing are employed. The red dots, blue squares and black solid line correspond to $\overline{v_\mathbf{n}H}$ on the left y-axis while the dashed red and blue lines correspond to simulation error on the right y-axis.

the outer radius set to ~~$R_\infty = 51$~~ $R_\infty = 15$ voxel with a voxel size of 18 µm, corresponding to inner and outer radii of 0.18 and 0.27 mm, respectively. In this way, the length scales of the test case are in a similar order of magnitude as the real microstructures considered later. Closed triangulated inner and outer sphere surfaces are created by applying the contour filter, which is subsequently passed as input to the CGAL volume meshing. A representation of the tetrahedral volume mesh obtained from CGAL and the corresponding triangular surface meshes are shown in Fig. 1b, where the volume mesh of the air space between the sphere has been left out for visual clarity. The slightly flattened regions on the sides of the sphere due to the original representation on a cubic lattice are still visible. The figure also reveals that the obtained CGAL mesh size is adaptive, i.e., in the vicinity of the interface, element sizes are reduced. After ~~computing the numerical solution of the Laplace equationon this geometry using Elmer,~~ solving the vapor equation, with appropriate boundary conditions, we obtain the interface velocity $v_\mathbf{n}$, shown in Fig. 1b. As expected, we observe a positive velocity on the inner shell, corresponding to vapor deposition, and a negative velocity on the outer shell, corresponding to sublimation. We then use our standard post-processing procedure ~~is used~~ to calculate the averaged growth rate $\overline{v_\mathbf{n}H}$ as an integral over the triangulated surface of the inner sphere with local curvatures and ~~growth~~ interface velocities as described previously in Sect. 3.2.2 and 3.3. Since we shall later focus on variations as a function of the ~~kinetic~~ condensation coefficient, we have repeated this procedure for ten different values of α. We also used two slightly different mesh quality parameters of the CGAL mesher to assess the sensitivity of the smoothness of the surface compared to the standard setup. The results of the validation are shown in Fig. 1c, yielding an excellent agreement of the numerical workflow with the analytical results for either smoothness. The results demonstrate

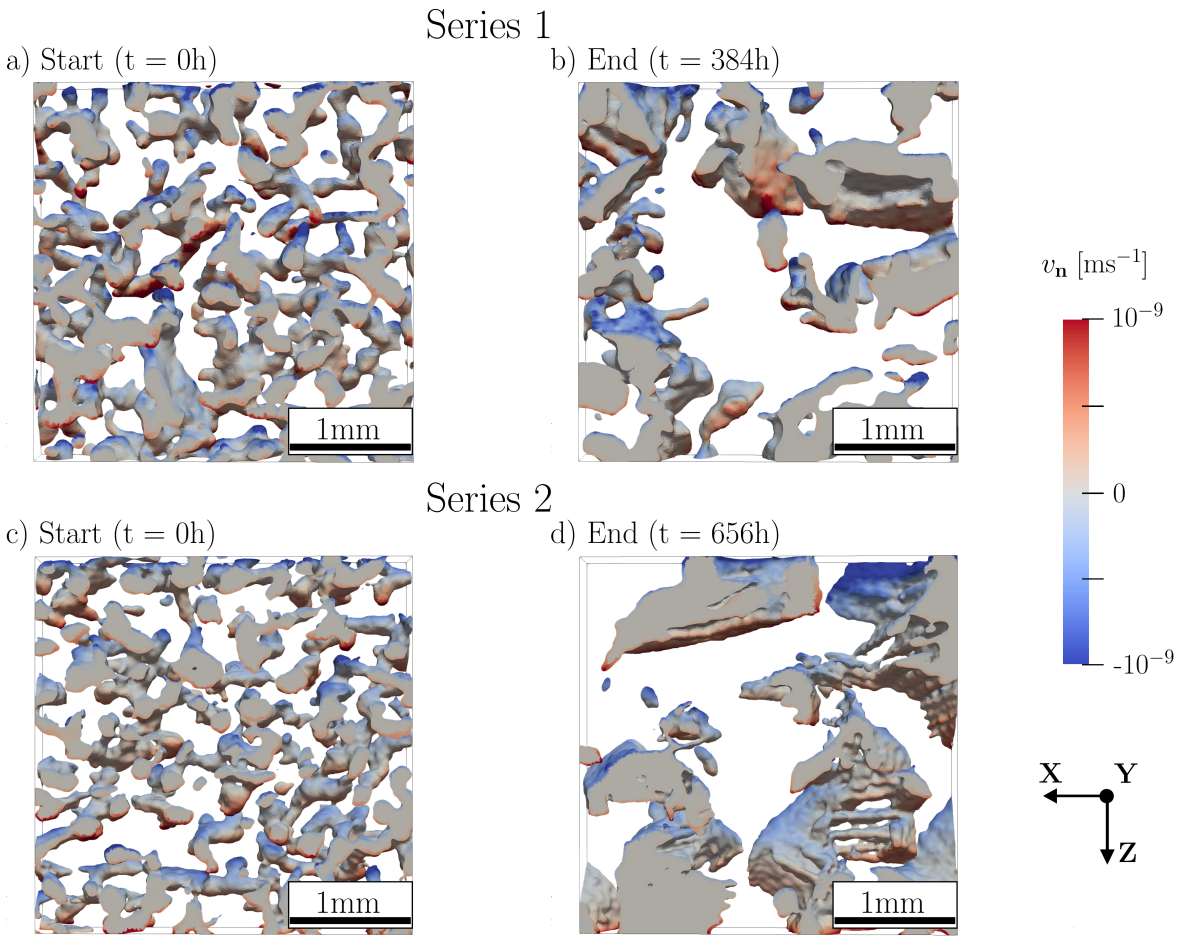

Figure 2. Evolution of the ice-air interface colored by ~~growth~~ interface velocity $v_\mathbf{n}$ demonstrated on cutouts of the length of 3.5 mm for a)/b) Series 1 and c)/d) Series 2.

that the choice of meshing and solver parameters leads to reliable numerical results. The agreement provides confidence in the correctness of the implementation of the entire workflow, which is now applied to the 4D image data of TGM.

4 Results

4.1 Overview

As an overview and for a visual inspection of the microstructures and the rates derived from the FE solution, we show in Fig. 2 the initial and the final microstructure of both experimental series, each colored by ~~growth~~ interface velocity $v_\mathbf{n}$ (computed using Eq. (17)). This reveals the morphological differences at the end of both experiments, where the longer experiment

(Series 2) has evolved into a more pronounced depth hoar state with enhanced formation of cup crystals (Pinzer et al., 2012). The simulations from Fig. 2 were carried out for the kinetic parameter $\alpha = 10^{-1}$ for Series 1 and $\alpha = 10^{-2.25}$ for Series 2 as showing the best ~~RMSE~~ root mean square error (RMSE) agreement in Fig 3c that is described in detail in the following section. As suggested by the analytical solution (Fig. 1c), or the sensitivity of the vapor fluxes by (Fourteau et al., 2021a), the simulated SSA rates are highly sensitive to the ~~kinetic coefficient~~ condensation coefficient α.

4.2 Coarse ~~time~~ temporal resolution modeling: ~~Kinetic coefficient~~ α estimation

In the first step, we compare the temporal evolution of the SSA s between experimental data and the model using a large time step for the modeled data. ~~This reduction in numerical effort allows us to perform a sensitivity study and estimate a value for the kinetic coefficient thatbest matches the experimental data. The results are shown in Fig. 3a, b. Time evolution of the SSA s experimental and modeled with a varying constant attachment kinetics coefficient α for a) Series 1 and b) Series 2. c) Root mean square error (RMSE) for the both series. We calculate the experimental and modeled data on the same ice-air interface obtained during the numerical procedure (see Sect. 3.2 and 3.3). The temporal resolution of experimental data is refined to $\Delta \approx 8$, i.e. the time step of two consecutive~~ For that, we downsample the experimental μCT images. ~~The modeled data are extracted~~ CT time series to match the coarse temporal resolution and only perform FE simulations on those. Specifically, the modeled SSA values are computed with a coarse time resolution of $\Delta = 48$ h for Series 1 (corresponding to 9 temporal points) and $\Delta \approx 60$ h for Series ~~2.~~ 2 (corresponding to 15 temporal points). This reduction in numerical effort allows us to perform a sensitivity study and estimate a value for the condensation coefficient α that best matches the experimental data. A fixed constant ~~attachment kinetics coefficient~~ α is used for each simulation. The range of α varies from 10^{-3} to 1 for Series 1 and from 10^{-3} to 10^{-1} for Series 2. ~~The~~ For the comparison with these simulated data, we simply use all available experimental SSA data (acquired for a temporal resolution of 8h). The results are shown in Fig. 3a,b. We note that a few simulation points are missing in Fig. 3, due the non-convergence of the FE solver. That being said, these missing points do not modify the overall decay of the simulated SSA time series. The best visual agreement between the experimental and modeled data is found for $\alpha^{\text{best}}_{\text{Series 1}} = 10^{-1}$ for Series 1 and $\alpha^{\text{best}}_{\text{Series 2}} = 10^{-2.25}$ for Series 2. For Series 1, the initial stage of the modeled curve with $\alpha^{\text{best}}_{\text{Series1}}$ is close to the experimental data, while the final stage significantly underestimates the observed SSA. The same trend can be seen in Series 2, less prominent though. The experimental data of Series 2 reveals significantly more fluctuations in the initial phase, which is naturally not captured by the coarse resolution modeling.

To assess the accuracy of modeled data quantitatively, the ~~root mean square error (RMSE)~~ RMSE is computed according to

$$\text{RMSE} = \sqrt{\frac{\sum_{n=1}^{N} (s^n_{\text{exp}} - s^n_{\text{mod}})^2}{N}} \tag{28}$$

where N is the number of time steps involved in the modeling. The results are shown in Fig. 3c. The minimum of the RMSE curve coincides with the best visual agreement, i.e., $\alpha^{\text{best}}_{\text{Series 1}} = 10^{-1}$, $\alpha^{\text{best}}_{\text{Series 2}} = 10^{-2.25}$. The difference between both optimal alpha values is one order of magnitude. Since the final stage of the modeled curve for Series 2 does not drop as much as for Series 1, the RMSE minimum for Series 2 is ~~deeper~~ lower despite higher data scattering.

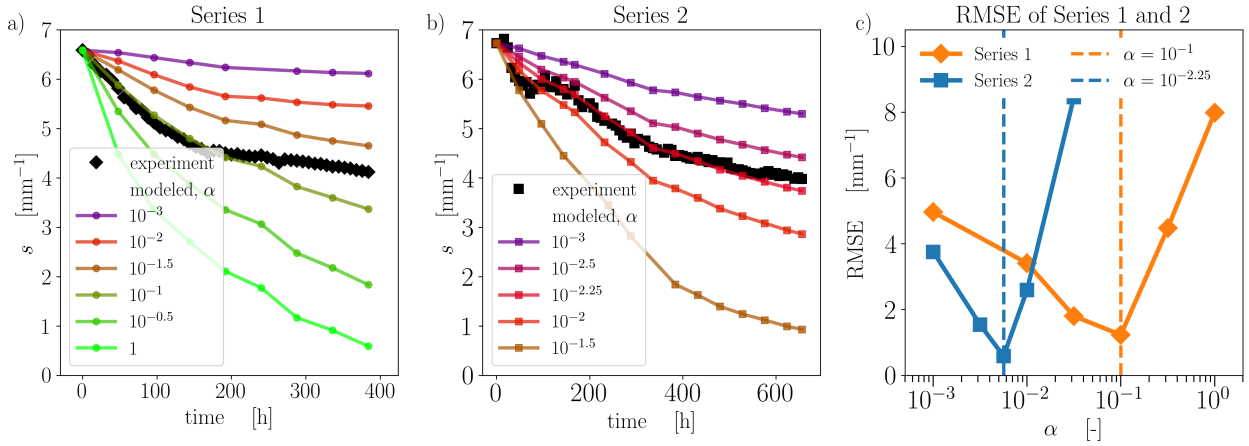

Figure 3. Time evolution of the SSA s experimental and modeled with a varying condensation coefficient α for a) Series 1 and b) Series 2. c) RMSE for the both series.

4.3 Impact of temporal resolution

To assess the impact of temporal resolution on the modeled decrease of SSA, we performed simulations with a time step refined down to the time interval between two μCT images, namely 8 h. Based on results from the previous subsection, the simulations for the fine temporal resolution are carried out for the ~~attachment kinetic~~ condensation coefficients $\alpha^{\text{best}}_{\text{Series 1}}$, $\alpha^{\text{best}}_{\text{Series 2}}$ that were obtained by RMSE optimization of the coarse resolution modeling. The results are given in Fig. 4. For Series 1, the fine resolution curve essentially coincides with the coarse one. The differences are slightly enhanced for Series 2, where the fine resolution curve lies slightly above the coarse one. The good agreement between the coarse and fine resolution simulations suggests that the coarse time step used in the previous section is sufficient to estimate the optimal α values.

These modeled SSA differences due to different temporal resolutions can now be further assessed through the error metric from Eq. (25). To this end, we fix the values of α to the optimal values found in the previous section and compute the SSA evolution for various temporal resolutions. We choose different numbers of time steps N such that our model provides the time evolution of the SSA $s(t_n)$ with $n = 1, 2, \ldots N$ for different ~~time~~ temporal resolutions Δ, Δ' where ~~$\Delta = t_N/N$~~ $\Delta = t_N/(N-1)$ (see Fig. 5a). On the one hand, this allows us to calculate the error metric from Eq. (25) using the model results alone. The results are shown in Fig. 5b as solid markers for the two series. On the other hand, the error metric can also be independently estimated using the stochastic error model of Eq. (26) for the given variance σ. Fitting the variance using the least squares method on the modeled data leads to values σ_{fit} = 0.0007 and 0.0006 for Series 1 and 2, respectively, and the results are shown in Fig. 5b as lines. These values are of the same order of magnitude as the variance computed as $\dot{s}/(2s)$ from the measurements: σ_{mes} = 0.0005 and 0.0007 for Series 1 and 2, respectively. Both estimations of the impact of the temporal resolution on the error metric are in reasonable agreement. Series 2 shows a significant difference in error between the coarsest

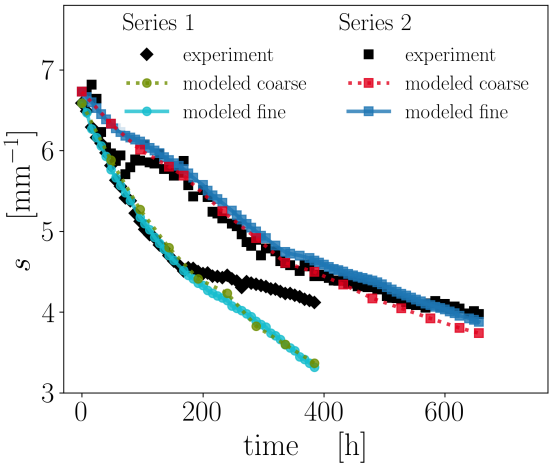

Figure 4. The time evolution of the SSA s for both series with coarse and fine temporal resolution for the best previously found values $\alpha^{\text{best}}_{\text{Series 1}}$, $\alpha^{\text{best}}_{\text{Series 2}}$.

and finest ~~time~~ temporal resolutions, both from simulations (red markers) or according to the μCT data (red line). On the contrary, the simulation-based estimation of Series 1 (blue markers) does not drop as much for the finest ~~time~~ temporal resolutions. This comes from the fact that the modeled SSA evolution using our finest and second-finest ~~time~~ temporal resolution substantially differ. Overall, the error metric's usage indicates that the ~~time~~ tempoal resolution's impact on the SSA evolution remains relatively small, with errors below 1%.

4.4 Signatures of a transition in ~~kinetic coefficients~~ α during TGM

Since we obtain a good agreement between experimental and modeled data for Series 1 only in the initial stage, additional simulations were conducted to explore this further. As previously shown in (cf. Krol and Löwe, 2018, Fig. 6), the Series 1 undergoes a morphological transition at around $t \approx$160 h, where up-facing and down-facing surfaces can be morphologically distinguished by their curvature distribution. From this time on, the second moment $\overline{H^2}$ of up-facing and down-facing surfaces split up to follow a different dynamics. Such a behavior during TGM is known from other work (Calonne et al., 2014a; Granger et al., 2021) and reflects the predominant emergence of facets on down-facing surfaces while the up-facing (subliming) surfaces remain rounded. Here, we show that this morphological transition during TGM is consistent with a transition in the ~~overall kinetic coefficient~~ effective condensation coefficient α that governs the SSA decay. To reveal the different kinetic behavior of Series 1 in the initial and final stages, we set the transition to $I(t_n), n \geq 20$, i.e. t = 160 h, and performed independent optimization of the ~~kinetic~~ condensation coefficient. Very good agreement with the coefficient of determination $R^2 = 0.99$ is achieved when the ~~kinetic~~ condensation coefficient is set to $\alpha = 10^{-1.5}$ for the final stage. The results for the optimal parameters are shown in Fig. 6a. While the transition is also present in Series 2 (Fig. 6 Krol and Löwe, 2018), it occurs

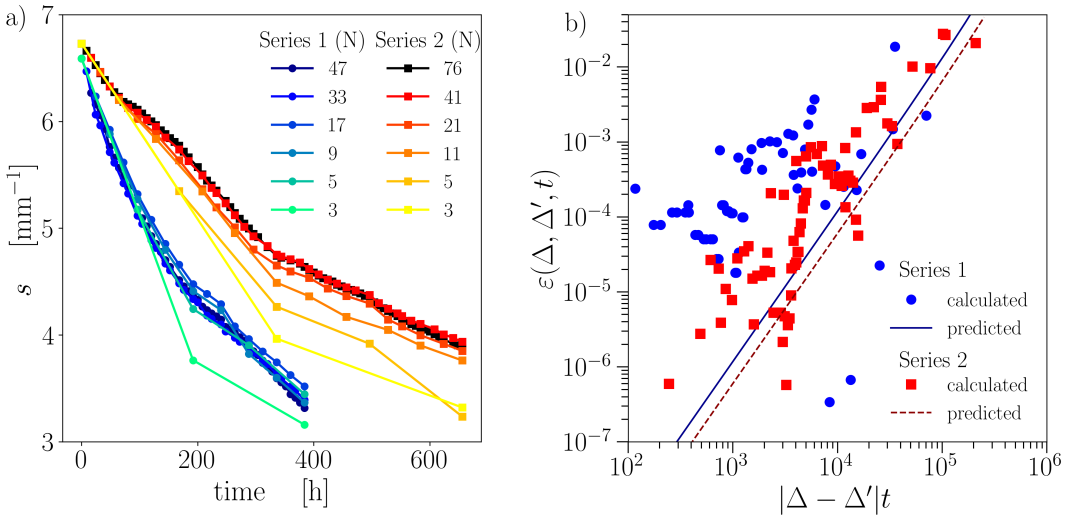

Figure 5. a) Different temporal resolutions of Series 1 and 2. b) The corresponding temporal resolution error ε calculated via Eqs. (25) and (26).

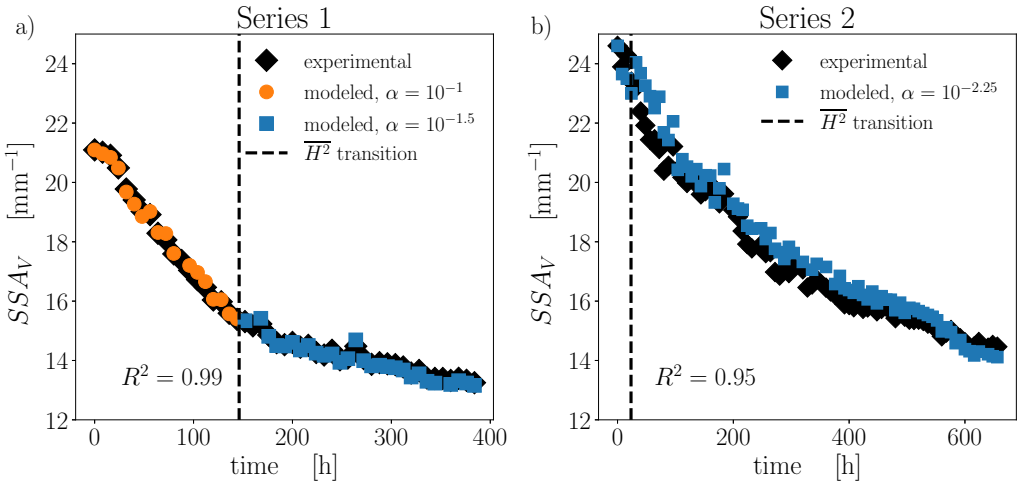

Figure 6. Comparison of experimental and modeled SSA time evolution. a) Series 1 with $\alpha^{\text{best}}_{\text{Series 1}}$ for $t \leq 160$ h and $\alpha = 10^{-1.5}$ for $t > 160$ h. b) Series 2 with $\alpha^{\text{best}}_{\text{Series 2}}$.

already very early in the time series after $t \approx 24$ h, cf. Fig. 6b. This is consistent with the observation that only one value of α is sufficient to match the measured data for Series 2. Since the initial stage in Series 2 is subject to higher fluctuations, an independent optimization of another α after a few time steps is inconclusive. Overall, this leads to the slightly reduced

coefficient of determination $R^2 = 0.95$ for Series 2. Fig. 6 summarizes the best possible match we obtained for the SSA in the highest resolution within the developed method.

5 Discussion

5.1 Modelling the SSA evolution from first principles

We have set up a numerical model that can simulate the evolution of one of snow's most fundamental microstructural parameters, the SSA, from 3D μCT images. The model is based on the established theoretical description of snow metamorphism through coupled ~~vapor and heat~~ heat and mass diffusion at the pore scale (Kaempfer and Plapp, 2009; Calonne et al., 2014b). The solution of the diffusion problem thereby extends previous work characterizing TGM from μCT images (Flin and Brzoska, 2008; Pinzer et al., 2012; Krol and Löwe, 2016), where vapor fluxes were estimated only within the assumption of local equilibrium at the interface. Under this assumption, fluxes can be estimated from temperature fields and curvatures alone without explicitly solving the vapor equation. Our diffusion model is essentially physically equivalent to (Kaempfer and Plapp, 2009) in the steady-state limit and has been used previously (Fourteau et al., 2021a).

The actual novelty of our work is the combination of the numerical solution of the heat and mass diffusion with the exact ~~evolution equation for the surface area~~ surface area evolution equation (Krol and Löwe, 2018). This combination allows us to rigorously validate the SSA dynamics without explicitly evolving the ice-air interface in 3D space. This approach is thus complementary to 4D microstructure evolution models such as (Kaempfer and Plapp, 2009) or (Bouvet et al., 2022). The advantage of including the surface area equation (Eq. (9)) into the analysis is the possibility of isolating the relevant ~~rate term~~ growth rate $\overline{v_\mathbf{n} H}$, either for constructing a stochastic error analysis (Sec. 3.4) or validation with analytical results (Sec. 3.5).

The model still requires considerable numerical resources, including volume meshing of the microstructure, the FE solution of ~~the heat and vapor~~ heat and mass diffusion equations taking into account kinetic effects of crystal growth, the extraction of the interface velocity $v_\mathbf{n}$ from the vapor field and the subsequent integration of the surface area equation. ~~As a result of the numerical effort~~Nevertheless, we were able to reproduce the decay of the SSA during TGM for the first time from "first principles", i.e. using a physical model and the actual microstructure without adjusting free parameters (in contrast to (Legagneux et al., 2004; Domine et al., 2007; Taillandier et al., 2007)). The only unknown (physical) parameter in the model is the ~~vapor attachment~~ condensation coefficient, which characterizes vapor deposition and sublimation kinetics.

5.2 The ~~kinetic~~ condensation coefficient α

We have demonstrated that the SSA evolution in the model is highly sensitive to the ~~kinetic coefficient~~ condensation coefficient α (see Fig. 3). The best agreement (see Fig. 6) is obtained for values of $10^{-3} < \alpha < 10^{-1}$ (slightly different for the two time series) that fall in the intermediate range (Fourteau et al., 2021a) of possible values. This intermediate range of kinetics is neither compatible with the assumption of slow kinetics underlying the homogenization from (Calonne et al., 2014b) nor the assumption of infinitely fast kinetics, which was previously used to compute $v_\mathbf{n}$ from local temperature gradients (Krol and

Löwe, 2016). While infinitely fast kinetics was already suggested to be inconsistent with the present experimental data sets (Krol and Löwe, 2018), this is now confirmed here from the estimated range for the values of α. From these results, we conclude that precise information about ~~the kinetic coefficient~~ α is essential and that modeling the SSA during TGM solely using geometry and temperatures/gradients and neglecting kinetic effects (Flanner and Zender, 2006) cannot be justified.

It is well known that α is difficult to measure experimentally. This is explained in (Libbrecht, 2005) and can be easily understood from Fig. 1c: When α is commonly measured through the inversion of ~~growth~~ interface velocity $v_\mathbf{n}$ data, the saturation form of the curve for the growth rate $\overline{v_\mathbf{n} H}$ as a function of α implies significant uncertainties on α even for minor errors in the growth rate in the saturation region, where diffusion dominates. Our methodology can be considered as a new (but similar) possibility of retrieving α by comparing simulated SSA evolution curves with experimental ones. From the reasoning given above, a high uncertainty should be expected. Surprisingly, the optimization (Fig. 3) reveals a rather sharp minimum. A similar procedure for obtaining α from the comparison of measured and modeled SSA curves was recently suggested by (Bouvet et al., 2022), where a value of $\alpha \approx 9.8 \times 10^{-4}$ was obtained from a comparison of a phase field model with experimental data in isothermal metamorphism. The latter work put forward an interesting alternative route to the optimization of α from experimental data by means of dimensional analysis. So, instead of conducting many simulations of different α (as done here), the same results could be obtained through non-dimensionalization and a single simulation. However, the temperature gradient case considered here is governed by two different time scales instead of only one in the isothermal case (Bouvet et al., 2022), which renders this approach less straightforward in our case. When comparing our results to other data, we see that the obtained values $10^{-1}, 10^{-1.5}$ for Series 1 and $10^{-2.25}$ for Series 2 lie in the commonly found range of $10^{-3} < \alpha < 10^{-1}$ (Libbrecht and Rickerby, 2013) which is also used by (Kaempfer and Plapp, 2009). They are slightly higher but in a similar order of magnitude as reported in (Fourteau et al., 2021a; Bouvet et al., 2022). In contrast, the ~~kinetic~~ condensation coefficient from Jafari et al. (2020) translates to $\alpha \approx 5 \cdot 10^{-7}$, which is significantly below this range.

In addition to the fact that both experimental series are apparently governed by a different ~~kinetic~~ condensation coefficient (Fig. 3), we have provided evidence (Fig. 6) that the ~~kinetic~~ condensation coefficient may even change during a single experiment. To comprehend this finding, we recall that in snow, different parts of the ice-air interface belong to different crystallographic orientations and habits (rounded vs. faceted). Both have different attachment mechanisms and, therefore, different α (Libbrecht, 2005). Using a single, constant value of α that does not vary over the surface (as done here) must be therefore understood as an *effective* kinetic coefficient. This effective coefficient can capture actual micro-scale variations of α since ~~still~~ a very good agreement for the SSA (as an integral property) ~~can be obtained. However~~is still obtained. It is quite remarkable that despite large variations of the condensation coefficient at the micro-scale, their collective behavior can be appropriately described through the use of a single α value. Indeed, in principle, the assumption of a constant α in Eq. 15 must be questioned on physical grounds. On facets, one expects that α is significantly reduced by orders of magnitude with a non-linear dependence on the ambient vapor field/supersaturation (Saito, 1996). Since facets cover only a fraction of the surface, this may explain why only a moderate drop in the effective α (Fig. 6) is observed instead. Further substantiation of this hypothesis in future work is feasible even without crystal orientation measurements such as (Granger et al., 2021). The surface area evolution equation (Eq. (9)) and the pore scale diffusion model can be easily extended to deal with spatially varying ~~kinetic~~ condensation

coefficients on the ice-air interface and corresponding surface area sub-classes (e.g., up-facing and down-facing). Such a setup would allow us to validate the hypothesis for the ~~kinetic~~ condensation coefficient transition here. Then it would be beneficial to include higher order interfacial properties like $\overline{H}$, $\overline{H^2}$ explicitly in the validation. This is, however, at the cost of evaluating higher order rate terms.

5.3 Propagation of measurement errors

Our analysis has shown why high-quality μCT data is crucial for our methodology. The complex numerical workflow contains several sources of errors that may affect the predicted SSA evolution. First, experimental input data have a limited spatial and temporal resolution, which leads to missing structural and interface correlations between two consecutive images. With a different experimental setup, such as in (Calonne et al., 2015) a higher spatial resolution may be achieved, though. Second, the ~~volume~~ volumes of interest considered here ~~for the simulations is~~ are relatively small, ~~which explains the noisy character~~ in particular for Series 2. This might lead to some non-representativeness issues and fluctuations in the measured SSA. This could explain the noisy nature of the experimental parameter curves. Third, all involved image analysis and simulation procedures come with additional numerical errors. While some uncertainties can be well controlled and assessed by testing the numerical workflow against analytical solutions (see Fig. 1), the existence of remaining errors is evident.

To address these errors and their impact on SSA modeling, we have exploited that the explicit SSA representation allows us to construct a stochastic error model (Sec. 3). This model predicts how the combination of temporal resolution Δ, observation time t, and methodological errors (subsumed in the variance σ of the μCT comparison data) affect the SSA prediction. The stochastic model is reasonably consistent with the observed convergence of the predictions under reduction of the time step (Fig. 5). The fact that errors can be quantitatively addressed even without knowing the true SSA is facilitated by the representation of the SSA as a differential equation (Eq. (9)). In the future, more sophisticated stochastic models should be envisaged and constructed from Eq. 9, which will further help to distinguish methodological noise and physics in the derived SSA dynamics.

5.4 Limitations and perspectives

Regarding model limitations besides the effective treatment of the ~~kinetic~~ condensation coefficient approach outlined above, we have neglected the latent heat term in the interface condition for the temperature equation (Eq. 6). This leads to a slightly simpler numerical situation where heat and vapor are coupled only one way, and the heat diffusion equation can be solved in advance. This strategy reduces the numerical cost of the method and facilitate the convergence of iterative solver used in the FE software. Despite this simplification, we still observe that the vapor solver ~~did not~~ had issues to converge for a few microstructures, which explains a few missing points in the modeled time series (e.g., ~~-~~Fig. ~~6). It~~ 4). The convergence of the FE simulations depends on the employed mesh and on the value of α. It could be facilitated by improving the mesh quality or increasing the maximum number of iterations. While this one-way coupling assumption eases the numerics, it was previously shown (Fourteau et al., 2021b) that for low density or fast kinetics, latent heat significantly contributes to the ~~volume averaged heat and mass fluxes~~ heat fluxes in snow and may thus likewise ~~enter~~ impact the volume averaged rate term $\overline{v_{\mathbf{n}} H}$. This should be carefully investigated for low-density μCT time series under TGM in the future, where the numerical solution will

become more demanding. In general, it would be advantageous to extend the analysis to other data sets. Here, we have used only two TGM time series which have been well studied before (Kaempfer et al., 2005; Pinzer et al., 2012; Krol and Löwe, 2018). Evaluation of high-resolution TGM experiments with systematic variations of the control parameters (microstructure, temperature, and temperature gradients) would be desirable. This would allow us to parameterize the relevant rate term $\overline{v_{\mathbf{n}} H}$ from the control parameters, which is the most promising way to proceed towards a physically based SSA equation in snow cover models.

6 Conclusions

We have addressed the SSA evolution in TGM within a rigorous framework that combines the surface area equation with pore-scale heat and mass diffusion simulations. The comparison to experimental μCT data allowed us to estimate effective ~~kinetic~~ condensation coefficients that led to good agreement of the simulations with the measurements without further adjustable parameters. This shows that the evolution of SSA can be understood from the first principles of pore-scale physics (diffusive heat and mass transports), provided that the ~~kinetic~~ effective condensation coefficient α is well-constrained. While this is a considerable step in understanding TGM our results highlight the importance of independent estimates of the ~~kinetic~~ condensation coefficient in snow, which is indispensable to proceed towards physically based SSA parameterizations in snow cover models.

Code and data availability. The data will be made available through envidat.ch upon acceptance of the manuscript.

Author contributions. A.B. and H.L designed the study. A.B. and K.F. wrote the code. A.B. performed numerical computations. A.B, K.F. and H.L. discussed the data and wrote the manuscript. H.L. received the funding and supervised the study.

Competing interests. The authors declare having no competing interests.

Acknowledgements. A.B. and H.L. would like to thank Prof. Dr. Michael Lehning for fruitful discussions. The project was funded by the Swiss National Science Foundation (SNSF) under grant no. 200020_178831. KF current position is funded by the European Research Council (ERC) under the European Union's Horizon 2020 research and innovation program (IVORI, grant no. 949516). We are thankful to Z.R. Courville and T. Kaempfer for reviewing the manuscript and to M. Niwano for editing it.

References

Adams, E. and Brown, R.: A model for crystal development in dry snow, Geophysical Research Letters, 9, 1287–1289, 1982.

Albert, M. and McGilvary, W.: Thermal effects due to air flow and vapor transport in dry snow, Journal of Glaciology, 38, 273–281, 1992.

Barrett, J. W., Garcke, H., and Nürnberg, R.: Numerical computations of faceted pattern formation in snow crystal growth, Physical Review E, 86, 011 604, 2012.

Bouvet, L., Calonne, N., Flin, F., and Geindreau, C.: Snow Equi-Temperature Metamorphism Described by a Phase-Field Model Applicable on Micro-Tomographic Images: Prediction of Microstructural and Transport Properties, Journal of Advances in Modeling Earth Systems, 14, e2022MS002 998, https://doi.org/10.1029/2022MS002998, e2022MS002998 2022MS002998, 2022.

Calonne, N., Flin, F., Morin, S., Lesaffre, B., du Roscoat, S. R., and Geindreau, C.: Numerical and experimental investigations of the effective thermal conductivity of snow, Geophysical research letters, 38, 2011.

Calonne, N., Flin, F., Geindreau, C., Lesaffre, B., and Rolland du Roscoat, S.: Study of a temperature gradient metamorphism of snow from 3-D images: time evolution of microstructures, physical properties and their associated anisotropy, The Cryosphere, 8, 2255–2274, 2014a.

Calonne, N., Geindreau, C., and Flin, F.: Macroscopic modeling for heat and water vapor transfer in dry snow by homogenization, The Journal of Physical Chemistry B, 118, 13 393–13 403, 2014b.

Calonne, N., Flin, F., Lesaffre, B., Dufour, A., Roulle, J., Puglièse, P., Philip, A., Lahoucine, F., Geindreau, C., Panel, J.-M., et al.: CellDyM: A room temperature operating cryogenic cell for the dynamic monitoring of snow metamorphism by time-lapse X-ray microtomography, Geophysical Research Letters, 42, 3911–3918, 2015.

Carslaw, H. S. and Jaeger, J. C.: Conduction of Heat in Solids, Oxford University Press, USA, 1986.

Colbeck, S.: Theory of metamorphism of dry snow, Journal of Geophysical Research: Oceans, 88, 5475–5482, https://doi.org/10.1029/JC088iC09p05475, 1983.

Coleou, C., Lesaffre, B., Brzoska, J.-B., Ludwig, W., and Boller, E.: Three-dimensional snow images by X-ray microtomography, Annals of glaciology, 32, 75–81, 2001.

Demange, G., Zapolsky, H., Patte, R., and Brunel, M.: A phase field model for snow crystal growth in three dimensions, npj Computational Materials, 3, 1–7, 2017.

Domine, F., Taillandier, A., Houdier, S., Parrenin, F., Simpson, W. R., and Douglas, T. A.: Interactions between snow metamorphism and climate: Physical and chemical aspects, Special Publication-Royal Society of Chemistry, 311, 27, 2006.

Domine, F., Taillandier, A.-S., and Simpson, W. R.: A parameterization of the specific surface area of seasonal snow for field use and for models of snowpack evolution, Journal of Geophysical Research: Earth Surface, 112, F02 031, https://doi.org/10.1029/2006JF000512, 2007.

Drew, D. A.: Evolution of geometric statistics, SIAM Journal on Applied Mathematics, 50, 649–666, 1990.

Dumont, M., Brun, E., Picard, G., Michou, M., Libois, Q., Petit, J., Geyer, M., Morin, S., and Josse, B.: Contribution of light-absorbing impurities in snow to Greenland's darkening since 2009, Nature Geoscience, 7, 509–512, 2014.

Ebner, P. P., Schneebeli, M., and Steinfeld, A.: Metamorphism during temperature gradient with undersaturated advective airflow in a snow sample, The Cryosphere, 10, 791–797, https://doi.org/10.5194/tc-10-791-2016, 2016.

Flanner, M. G. and Zender, C. S.: Linking snowpack microphysics and albedo evolution, Journal of Geophysical Research: Atmospheres, 111, D12 208, 2006.

Flin, F. and Brzoska, J.-B.: The temperature-gradient metamorphism of snow: vapour diffusion model and application to tomographic images, Annals of Glaciology, 49, 17–21, 2008.

Flin, F., Brzoska, J.-B., Lesaffre, B., Coléou, C., and Pieritz, R. A.: Three-dimensional geometric measurements of snow microstructural evolution under isothermal conditions, Annals of glaciology, 38, 39–44, 2004.

Fourteau, K., Domine, F., and Hagenmuller, P.: Macroscopic water vapor diffusion is not enhanced in snow, The Cryosphere, 15, 389–406, https://doi.org/10.5194/tc-15-389-2021, 2021a.

Fourteau, K., Domine, F., and Hagenmuller, P.: Impact of water vapor diffusion and latent heat on the effective thermal conductivity of snow, The Cryosphere, 15, 2739–2755, 2021b.

Granger, R., Flin, F., Ludwig, W., Hammad, I., and Geindreau, C.: Orientation selective grain sublimation–deposition in snow under temperature gradient metamorphism observed with diffraction contrast tomography, The Cryosphere, 15, 4381–4398, https://doi.org/10.5194/tc-15-4381-2021, 2021.

Hagenmuller, P., Matzl, M., Chambon, G., and Schneebeli, M.: Sensitivity of snow density and specific surface area measured by microtomography to different image processing algorithms, The Cryosphere, 10, 1039–1054, https://doi.org/10.5194/tc-10-1039-2016, 2016.

Hammonds, K., Lieb-Lappen, R., Baker, I., and Wang, X.: Investigating the thermophysical properties of the ice–snow interface under a controlled temperature gradient: Part I: Experiments & Observations, Cold Regions Science and Technology, 120, 157–167, 2015.

Hanot, L. and Dominé, F.: Evolution of the Surface Area of a Snow Layer, Environmental Science & Technology, 33, 4250–4255, https://doi.org/10.1021/es9811288, 1999.

Harris Stuart, R., Faber, A.-K., Wahl, S., Hörhold, M., Kipfstuhl, S., Vasskog, K., Behrens, M., Zuhr, A. M., and Steen-Larsen, H. C.: Exploring the role of snow metamorphism on the isotopic composition of the surface snow at EastGRIP, The Cryosphere, 17, 1185–1204, https://doi.org/10.5194/tc-17-1185-2023, 2023.

Hobbs, P.: Ice Physics, Oxford Classic Texts in the Ph, OUP Oxford, 2010.

Jafari, M., Gouttevin, I., Couttet, M., Wever, N., Michel, A., Sharma, V., Rossmann, L., Maass, N., Nicolaus, M., and Lehning, M.: The Impact of Diffusive Water Vapor Transport on Snow Profiles in Deep and Shallow Snow Covers and on Sea Ice, Frontiers in Earth Science, 8, 249, https://doi.org/10.3389/feart.2020.00249, 2020.

Jafari, M., Sharma, V., and Lehning, M.: Convection of water vapour in snowpacks, Journal of Fluid Mechanics, 934, A38, https://doi.org/10.1017/jfm.2021.1146, 2022.

Kaempfer, T. U. and Plapp, M.: Phase-field modeling of dry snow metamorphism, Physical Review E, 79, 031 502, 2009.

Kaempfer, T. U., Schneebeli, M., and Sokratov, S. A.: A microstructural approach to model heat transfer in snow, Geophysical Research Letters, 32, 21, https://doi.org/10.1029/2005GL023873, 2005.

Krol, Q. and Löwe, H.: Analysis of local ice crystal growth in snow, Journal of Glaciology, 62, 378–390, 2016.

Krol, Q. and Löwe, H.: Upscaling ice crystal growth dynamics in snow: Rigorous modeling and comparison to 4D X-ray tomography data, Acta Materialia, 151, 478–487, 2018.

Legagneux, L., Taillandier, A.-S., and Domine, F.: Grain growth theories and the isothermal evolution of the specific surface area of snow, Journal of applied physics, 95, 6175–6184, 2004.

Li, Y. and Baker, I.: Metamorphism observation and model of snow from summit, Greenland under both positive and negative temperature gradients in a micro computed tomography, Hydrological Processes, 36, e14 696, https://doi.org/10.1002/hyp.14696, 2022.

Libbrecht, K. G.: The physics of snow crystals, Reports on progress in physics, 68, 855, 2005.

Libbrecht, K. G. and Rickerby, M. E.: Measurements of surface attachment kinetics for faceted ice crystal growth, Journal of crystal growth, 377, 1–8, 2013.

Malinen, M. and Råback, P.: Elmer finite element solver for multiphysics and multiscale problems, Multiscale Model. Methods Appl. Mater. Sci., 19, 101–113, 2013.

Matzl, M. and Schneebeli, M.: Measuring specific surface area of snow by near-infrared photography, Journal of Glaciology, 52, 558–564, https://doi.org/10.3189/172756506781828412, 2006.

Miller, D. and Adams, E.: A microstructural dry-snow metamorphism model for kinetic crystal growth, Journal of Glaciology, 55, 1003–1011, 2009.

Picard, G., Löwe, H., and Mätzler, C.: Brief communication: A continuous formulation of microwave scattering from fresh snow to bubbly ice from first principles, The Cryosphere, 16, 3861–3866, 2022.

Pinzer, B. and Schneebeli, M.: Breeding snow: an instrumented sample holder for simultaneous tomographic and thermal studies, Measurement Science and Technology, 20, 095 705, 2009a.

Pinzer, B. R. and Schneebeli, M.: Snow metamorphism under alternating temperature gradients: Morphology and recrystallization in surface snow, Geophysical Research Letters, 36, 23, https://doi.org/10.1029/2009GL039618, 2009b.

Pinzer, B. R., Schneebeli, M., and Kaempfer, T. U.: Vapor flux and recrystallization during dry snow metamorphism under a steady temperature gradient as observed by time-lapse micro-tomography, The Cryosphere, 6, 1141–1155, https://doi.org/10.5194/tc-6-1141-2012, 2012.

Pokrifka, G. F., Moyle, A. M., Hanson, L. E., and Harrington, J. Y.: Estimating Surface Attachment Kinetic and Growth Transition Influences on Vapor-Grown Ice Crystals, Journal of the Atmospheric Sciences, 77, 2393 – 2410, https://doi.org/10.1175/JAS-D-19-0303.1, 2020.

Saad, Y.: Iterative Methods for Sparse Linear Systems, Society for Industrial and Applied Mathematics, 2003.

Saito, Y.: Statistical physics of crystal growth, World Scientific, 1996.

Schleef, S. and Loewe, H.: X-ray microtomography analysis of isothermal densification of new snow under external mechanical stress, Journal of Glaciology, 59, 233–243, 2013.

Schleef, S., Löwe, H., and Schneebeli, M.: Influence of stress, temperature and crystal morphology on isothermal densification and specific surface area decrease of new snow, The Cryosphere, 8, 1825–1838, https://doi.org/10.5194/tc-8-1825-2014, 2014.

Schneebeli, M. and Sokratov, S. A.: Tomography of temperature gradient metamorphism of snow and associated changes in heat conductivity, Hydrological Processes, 18, 3655–3665, 2004.

Schroeder, W., Martin, K., and Lorensen, B.: The visualization toolkit, 4th edn. Kitware, New York, 2006.

Schweizer, J., Bruce Jamieson, J., and Schneebeli, M.: Snow avalanche formation, Reviews of Geophysics, 41, 4, 2003.

Shreve, R.: Migration of air bubbles, vapor figures, and brine pockers in ice under a temperature gradient, Journal of Geophysical Research, 72, 4093–4100, 1967.

Taillandier, A.-S., Domine, F., Simpson, W. R., Sturm, M., and Douglas, T. A.: Rate of decrease of the specific surface area of dry snow: Isothermal and temperature gradient conditions, Journal of Geophysical Research: Earth Surface, 112, F3, 2007.

The CGAL Project: CGAL User and Reference Manual, CGAL Editorial Board, 5.5.1 edn., https://doc.cgal.org/5.5.1/Manual/packages.html, 2022.

Van der Vorst, H. A.: Bi-CGSTAB: A fast and smoothly converging variant of Bi-CG for the solution of nonsymmetric linear systems, SIAM Journal on scientific and Statistical Computing, 13, 631–644, 1992.

Wang, X. and Baker, I.: Observation of the microstructural evolution of snow under uniaxial compression using X-ray computed microtomography, Journal of Geophysical Research: Atmospheres, 118, 12,371–12,382, https://doi.org/https://doi.org/10.1002/2013JD020352, 2013.

Wang, X. and Baker, I.: Evolution of the specific surface area of snow during high-temperature gradient metamorphism, Journal of Geophysical Research: Atmospheres, 119, 13–690, https://doi.org/10.1002/2014JD022131, 2014.

Wiese, M. and Schneebeli, M.: Snowbreeder 5: a Micro-CT device for measuring the snow-microstructure evolution under the simultaneous influence of a temperature gradient and compaction, Journal of Glaciology, 63, 355–360, 2017.

Zermatten, E., Schneebeli, M., Arakawa, H., and Steinfeld, A.: Tomography-based determination of porosity, specific area and permeability of snow and comparison with measurements, Cold Regions Science and Technology, 97, 33–40, https://doi.org/10.1016/j.coldregions.2013.09.013, 2014.